
**This is an electronic reprint of the original article.
This reprint *may differ* from the original in pagination and typographic detail.**

Author(s): Boéré, René; Chivers, Tristram; Roemmele, Tracey; Tuononen, Heikki

Title: Electrochemical and Electronic Structure Investigations of the $[S_3N_3]^\bullet$ Radical and Kinetic Modeling of the $[S_4N_4]_n/[S_3N_3]_n$ ($n = 0, -1$) Interconversion

Year: 2009

Version:

Please cite the original version:

Boéré, R., Chivers, T., Roemmele, T., & Tuononen, H. (2009). Electrochemical and Electronic Structure Investigations of the $[S_3N_3]^\bullet$ Radical and Kinetic Modeling of the $[S_4N_4]_n/[S_3N_3]_n$ ($n = 0, -1$) Interconversion. *Inorganic Chemistry*, 48(15), 7294-7306.
<https://doi.org/10.1021/ic900742q>

All material supplied via JYX is protected by copyright and other intellectual property rights, and duplication or sale of all or part of any of the repository collections is not permitted, except that material may be duplicated by you for your research use or educational purposes in electronic or print form. You must obtain permission for any other use. Electronic or print copies may not be offered, whether for sale or otherwise to anyone who is not an authorised user.

Electrochemical and Electronic Structure Investigations of the $[\text{S}_3\text{N}_3]^{\cdot}$ Radical and Kinetic Modeling of the $[\text{S}_4\text{N}_4]^n/[\text{S}_3\text{N}_3]^n$ ($n = 0, -1$) Interconversion

René T. Boéré,^{†*} Tristram Chivers,^{§*} Tracey L. Roemmele^{†§} and Heikki M. Tuononen[‡]

[†] *Department of Chemistry and Biochemistry, University of Lethbridge, Lethbridge, Alberta, Canada T1K 3M4.*

[§] *Department of Chemistry, University of Calgary, Calgary, Alberta, Canada T2N 1N4.*

[‡] *Department of Chemistry, University of Jyväskylä, Jyväskylä, FI-40014, Finland.*

* To whom correspondence may be addressed. (R. T. Boéré: Tel. (403) 329-2045, Fax (403) 329-2057, E-mail: boere@uleth.ca; T. Chivers: Tel. (403) 220-5741, Fax (403) 289-9488, E-mail: chivers@ucalgary.ca).

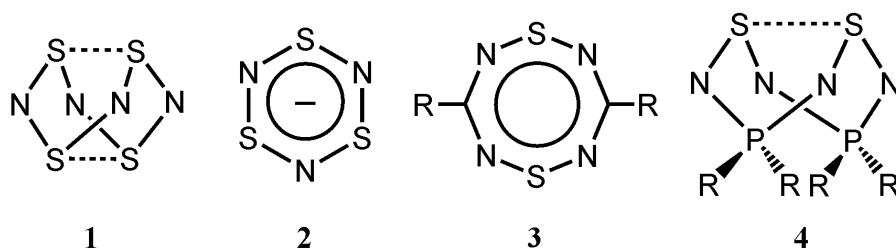
Abstract

Voltammetric studies of S_4N_4 employing both cyclic (CV) and rotating disk (RDE) methods in CH_2Cl_2 at a glassy carbon electrode reveal a one-electron reduction at -1.00 V (versus ferrocene/ferrocenium), which produces a second redox couple at -0.33 V, confirmed to be the electrochemically generated $[S_3N_3]^-$ by CV studies on its salts. Diffusion coefficients (CH_2Cl_2 / 0.4 M $[nBu_4N][PF_6]$) estimated by RDE methods: S_4N_4 , $1.17 \times 10^{-5} \text{ cm}^2 \text{ s}^{-1}$; $[S_3N_3]^-$, $4.00 \times 10^{-6} \text{ cm}^2 \text{ s}^{-1}$. Digital simulations of the CVs detected slow rates of electron transfer for both couples and allowed for a determination of rate constants for homogeneous chemical reaction steps subsequent to electron transfer. The common parameters ($k_{f1} = 2.0 \pm 0.5 \text{ s}^{-1}$, $k_{s1} = 0.034 \pm 0.004 \text{ s}^{-1}$ for $[S_4N_4]^{-/0}$; $k_{f2} = 0.4 \pm 0.2 \text{ s}^{-1}$, $k_{s2} = 0.022 \pm 0.005 \text{ s}^{-1}$ for $[S_3N_3]^{-/0}$ at $T = 21 \pm 2^\circ\text{C}$) fit well to a "square-scheme" mechanism over the entire range of data with first order decay of both redox products. An alternate model could also be fit wherein $[NS]^\bullet$ liberated in the first step reacts with formed $[S_3N_3]^\bullet$ to reproduce S_4N_4 with an apparent second order rate constant $k_{f2}' = 1.1 \pm 0.3 \times 10^3 \text{ M}^{-1} \text{ s}^{-1}$. The crystal structure of $[PPN][S_3N_3]$ was determined by X-ray crystallography indicating the solvation of the anion by one equivalent of methanol. The generated $[S_4N_4]^{-\bullet}$ radical anion was detected by the Simultaneous Electrochemical Electron Paramagnetic Resonance (SEEPR) method to give: (a) $[^{32}S_4^{14}N_4]^{-\bullet}$, 9 lines, $a(^{14}N) = 0.118 \text{ mT}$; (b) $[^{32}S_4^{15}N_4]^{-\bullet}$ 5 lines, $a(^{15}N) = 0.164 \text{ mT}$; (c) $[^{33}S_4^{14}N_4]^{-\bullet}$, *estimated* $a(^{14}N) = 0.118$, $a(^{33}S) = 0.2 \text{ mT}$; $g = 2.0008(1)$. Equivalence of ^{33}S hyperfine splittings is consistent with dynamic averaging of the C_{2v} geometry in solution. High-level electronic structure calculations provide convincing evidence for an open-shell doublet triradicaloid character to the ground state wave function of $[S_3N_3]^\bullet$.

Introduction

Unsaturated binary sulfur–nitrogen compounds readily undergo redox reactions that are accompanied by remarkable structural changes, which continue to challenge the emerging understanding of mechanistic pathways in main group chemistry.¹ Despite being formally electron-rich they are often capable of being either oxidized or reduced.² Tetrasulfur tetranitride, S_4N_4 (**1**), is the best known member of this class and has been extensively investigated by electrochemistry, EPR spectroscopy and DFT calculations.³ Its versatility stems from multifaceted chemical behavior whereby it is the source of many other binary sulfur-nitrogen (S,N) compounds, including the cyclic trisulfur trinitride anion $[S_3N_3]^-$ (**2**).⁴

Chart 1. Chemical Structures for Compounds **1–4**.



The redox chemistry of S_4N_4 has been the subject of numerous studies.¹ Chemical oxidation with reagents such as AsF_5 or HSO_3F produces the cyclic $[S_3N_2]^{+\bullet}$ radical cation⁵ or, in the presence of an excess of the oxidizing agents $SbCl_5$, AsF_5 or $S_2O_6F_2$, the cyclic dication $[S_4N_4]^{2+}$.⁶ The radical cation $[S_4N_4]^{+\bullet}$ has not been convincingly characterized. The EPR spectrum of the radical formed on γ -irradiation of S_4N_4 in $CFCl_3$ at 77 K was attributed to $[S_4N_4]^{+\bullet}$, but no ^{14}N hyperfine splitting (hfs) was observed.^{7a} A minor product from the reaction of $(NSCl)_3$ with $FeCl_3$ in CH_2Cl_2 was identified as $[S_4N_4]^{+\bullet}[FeCl_4]^-$ on the basis of the X-ray structure;⁷ however, the perturbation of the S–N bond lengths in the eight-membered ring is consistent with the formation of the protonated species $[S_4N_4H]^+$.⁸ Ring-size changes also

accompany the oxidation of S_4N_4 with Cl_2 or SO_2Cl_2 to $S_3N_3Cl_3$ while reduction of the latter reproduces S_4N_4 .¹

Bojes and Chivers provided convincing evidence that the electrolytic reduction of S_4N_4 in anhydrous ethanol produced salts of $[S_3N_3]^-$, while the end product of reduction with potassium metal in dimethoxyethane (DME) is $K[S_3N_3]$.^{4b} Previously, Chapman and Massey had reported a surprisingly persistent EPR signal from potassium metal reduction of S_4N_4 in DME at room temperature. They observed a nine-line pattern with the intensity ratio expected from hfs of 0.322 mT to four equivalent $I = 1$ nuclei, which was attributed to the radical anion $[S_4N_4]^{•-}$.^{3a} However, this assignment has been refuted by the work of Meinzer *et al.*^{3b} and Williford *et al.*^{3c} who both reported the generation of a transient EPR signal during low-temperature electrochemical reduction of S_4N_4 in THF/ $[nBu_4N][ClO_4]$ at $-25\text{ }^\circ\text{C}$ or $CH_3CN/[Et_4N][ClO_4]$ at $-20\text{ }^\circ\text{C}$ with a much smaller hfs reported to be 0.1185(1) or 0.117(2) mT. In contrast to the 1962 report, neither of the electrochemical studies gave a detectable radical at room temperature; the true origin of the 0.322 mT nine-line pattern thus remains a mystery. Williford *et al.*^{3c} also performed a variable-temperature cyclic voltammetry (CV) study in $CH_3CN/[Et_4N][ClO_4]$ over the range $-25\text{ }^\circ\text{C}$ to $-3\text{ }^\circ\text{C}$ that provides additional support for the assignment of their EPR spectrum to $[S_4N_4]^{•-}$.

Exhaustive polarographic^{3d,e,f} and coulometric^{3e,9} studies on S_4N_4 have confirmed the initial one-electron reduction process at room temperature. The final products of reduction in aprotic solvents are salts of $[S_3N_3]^-$ that appear to be produced quantitatively with the uptake of $1.3\text{ }e^-$ per S_4N_4 . Coulometric reduction in the presence of proton donors (acetic or monochloroacetic acids) yields the tetraimide $S_4N_4H_4$.^{3d} The electrochemical oxidation of $[S_3N_3]^-$ (as the Et_4N^+ salt in $CH_3CN/[Et_4N][ClO_4]$) produces S_4N_4 almost quantitatively;^{3e} however, attempts to detect a

radical upon electrolytic oxidation of [PPN][S₃N₃] in CH₂Cl₂ by EPR spectroscopy were unsuccessful.¹⁰ Very recently the photochemistry of S₄N₄ was investigated in Ar matrices, demonstrating the facile interconversion of S₄N₄ to different isomers.¹¹ Three intermediates were identified with the aid of DFT calculations, two of which are novel S₃N₃ rings carrying exocyclic (N)–S≡N or (S)–N=S groups. These two bear a strong resemblance to species postulated in this work for the decay of [S₄N₄]^{•-} and may be directly involved in the coupling of neutral [NS][•] with [S₃N₃][•].

We recently reported¹² the first identification of the radical anions of unsaturated C₂N₄S₂ (**3**) and P₂N₄S₂ (**4**) rings by using an in situ electrochemical cell capable of Simultaneous Electrochemical Electron Paramagnetic Resonance (SEEPR)¹³ spectroscopy, as well as an investigation of the mechanism of their decomposition by a kinetic analysis employing modern digital simulation of CVs. In connection with our interest in the characterization of short-lived, binary S,N radicals,¹⁴ we now report the application of these methods to detailed investigations of (a) the reduction of S₄N₄ and (b) the oxidation of [S₃N₃]⁻. In part (a) we have used the SEEPR technique to acquire high quality EPR spectra of the anion radical [S₄N₄]^{•-} using natural abundance, ¹⁵N and ³³S-enriched S₄N₄ at low temperature. We have also employed digital simulations of CVs to provide insights into the nature of the S₄N₄ ↔ [S₃N₃]⁻ interconversion. The target of part (b) was [S₃N₃][•] in condensed phases; this radical has previously only been detected in the vapors of (SN)_x by photoelectron spectroscopy.¹⁵ The [S₃N₃][•] radical has also been invoked as an intermediate in the formation of [S₃N₃]⁻ salts from the ten-membered ring [S₅N₅]Cl via ring contraction.^{16a} Interestingly, the compound [PhCN₂S₂][S₃N₃], which can be obtained by the reaction of the dimer (PhCN₂S₂)₂ with the vapors formed from (SN)_x at 160 °C, is described as a biradical [PhCN₂S₂][•][S₃N₃][•] rather than an ionic compound on the basis of *ab*

initio molecular orbital calculations.^{16a} However, single-crystal EPR studies could detect only ~1% $[\text{PhCN}_2\text{S}_2]^{\bullet}$ trapped in a matrix of what seems to be $[\text{PhCN}_2\text{S}_2]^+[\text{S}_3\text{N}_3]^-$.^{16b} Surprisingly, despite the apparent solubility of this adduct in common solvents, no solution-phase EPR evidence which could corroborate the biradical nature of this compound was reported. In pursuit of the elusive $[\text{S}_3\text{N}_3]^{\bullet}$ radical we have carried out a detailed CV and SEEPR study of the oxidation of the $[\text{S}_3\text{N}_3]^-$ anion in the form of the known $[\text{Cp}_2\text{Co}]^+$ and $[\text{PPN}]^+$ ($\text{PPN} = [(\text{Ph}_3\text{P})_2\text{N}]^+$) salts.^{4d,17} The X-ray structure of the $[\text{PPN}]^+$ salt is also described. These experimental investigations are supplemented by high-level theoretical calculations of the electronic structure of $[\text{S}_3\text{N}_3]^{\bullet}$.

Experimental

Reagents and General Procedures. S_4N_4 ,^{3k,1} as well as the ^{15}N and ^{33}S isotope-labeled analogues,¹⁸ $[\text{Cp}_2\text{Co}][\text{S}_3\text{N}_3]$ ¹⁷ and $[\text{PPN}][\text{S}_3\text{N}_3]$ ^{4d-e, 19} were obtained by literature methods. The isotopic purity of 99.9 % $^{33}\text{S}_4^{14}\text{N}_4$ was confirmed using LRMS: 187.9 ($^{33}\text{S}_4^{14}\text{N}_4^+$, 2 %); 140.9 ($^{33}\text{S}_3^{14}\text{N}_3^+$, 13 %); 93.9 ($^{33}\text{S}_2^{14}\text{N}_2^+$, 19 %); 47.0 ($^{33}\text{S}^{14}\text{N}^+$, 100 %). Dichloromethane and acetonitrile (BDH, reagent grade) were purified by distillation (CH_3CN : first from P_2O_5 , then CaH_2 , CH_2Cl_2 : from CaH_2). Both solvents were purged with dry nitrogen prior to use. Electrochemical grade tetrabutylammonium hexafluorophosphate $[\text{nBu}_4\text{N}][\text{PF}_6]$ (Fluka) was used as the supporting electrolyte and was stored in a dessicator. Ferrocene (Fc) was sublimed prior to use.

Voltammetry. Cyclic voltammograms were obtained at 20 ± 2 °C in both CH_3CN and CH_2Cl_2 solutions containing 0.1 M and 0.4 M $[\text{nBu}_4\text{N}][\text{PF}_6]$, respectively, as the supporting electrolyte. These solutions were purged with dry nitrogen for 10 min directly before use, and were kept under a blanket of nitrogen during all experiments. CVs, bulk electrolysis, and rotating disk

electrode (RDE) measurements were performed with a Princeton Applied Research PARSTAT 2273 potentiostat in conjunction with a PINE Model AFMSRXE Modulated Speed Rotator. The voltammetry cell design has been described previously.¹² The cell used for RDE measurements replaced the central size-10 joint with a 60×15 mm cylinder to accommodate the rotating electrode. Initial background scans characterized the size of the accessible electrochemical window and provided an estimate of the likely background current. The CVs were obtained over scan rates of 0.05–20 V s⁻¹. The potentials for S₄N₄ and [PPN][S₃N₃] are reported vs. the operative formal potential, $E_{Fc^{0/+}}^{0/}$, for the Fc/Fc⁺ redox couple, which was used as an internal standard. Potentials for [Cp₂Co][S₃N₃] are also quoted vs. ferrocene, for which the cobaltocene/cobaltocenium redox couple is known to appear at –1.35 V in dichloromethane.²⁰ The 3.0 mm BASi glassy carbon (GC) working electrode area (6.6 x 10⁻² cm²) was determined from the peak current value obtained for the reversible one-electron reduction of ferrocene (1.0 mM, 2.0 mM, and 3.0 mM solutions) in CH₃CN (0.1 M [nBu₄N][PF₆]) under conditions of CV and using the Randles-Sevcik equation:²¹

$$I_p = 0.4463nF \left(\frac{nF}{RT} \right)^{1/2} AD^{1/2} \nu^{1/2} C \quad (1)$$

where I_p is the peak current (A), n (the number of electrons in the charge-transfer process) is taken to be 1.0, A is the electrode area (cm²), D is the diffusion coefficient (taken to be 2.3 x 10⁻⁵ cm² s⁻¹),²¹ C is the concentration (mol cm⁻³), ν is the scan rate (V s⁻¹), and the other symbols have their usual meanings. The working electrode was polished with an Al₂O₃ (Buehler, 0.05 μm) slurry on a clean polishing cloth, rinsed with distilled water, and dried with tissue paper prior to use. A 5.0 mm diameter GC macrodisk electrode (area = 1.86 x 10⁻¹ cm²) obtained from

Pine Instruments was employed for RDE voltammetry. Diffusion coefficients were determined from limiting current values obtained from RDE voltammetry and use of the Levich equation:²¹

$$I_l = 0.62nFAD_o^{2/3}\omega^{1/2}\nu_k^{-1/6}C_o^* \quad (2)$$

where I_l is the limiting current, ω is the angular frequency of rotation (s^{-1}), (ν_k) is the kinematic viscosity and the other symbols have been described above. Values for kinematic viscosity at 20 °C were taken to be those for the pure solvents: 0.004536 $cm^2 s^{-1}$ for CH_3CN ²² and 0.003318 $cm^2 s^{-1}$ for CH_2Cl_2 .²² The almost linear plots of the I_p^{c1} vs. $\nu^{1/2}$ obtained for the first reduction process in S_4N_4 , as well as of I_p^{a2} vs. $\nu^{1/2}$ for the first oxidation process in $[S_3N_3]^-$ in CH_2Cl_2 at a GC working electrode implies that the mass transport process at the peak potential is controlled by diffusion in both cases. From the Randles-Sevcik relationship (Eqn. 1) an estimation of the diffusion coefficients was also obtained from straight line fits to the I_p^{c1} vs. $\nu^{1/2}$ and I_p^{a2} vs. $\nu^{1/2}$ plots, respectively.

Table 1. Diffusion Coefficient Values for S_4N_4 and $[S_3N_3]^-$ in CH_2Cl_2 at $T = 21 \pm 2$ °C

Method	Electrode	RPM	$D (S_4N_4) / 10^{-5} cm^2$	$D ([S_3N_3]^-) / 10^{-5} cm^2$
RDE^a				
CH_2Cl_2	GC	2250	1.20 ^b	0.406 ^c
CH_2Cl_2	GC	2000	1.20 ^b	0.408 ^c
CH_2Cl_2	GC	1750	1.20 ^b	0.408 ^c
CH_2Cl_2	GC	1500	1.20 ^b	0.406 ^c
CH_2Cl_2	GC	1250	1.21 ^b	0.408 ^c
CH_2Cl_2	GC	1000	1.22 ^b	0.408 ^c
RDE (Koutecky-Levich)^d				
CH_2Cl_2	GC	—	1.26 ^b	0.411 ^c
CH_2Cl_2	GC	—	1.11 ^e	0.402 ^f
CV^d				
CH_2Cl_2	GC	—	0.96 ^g	0.34 ^h

^a 0.4 M [nBu_4N][PF₆], $\nu = 0.01$ V s^{-1} . ^b 3.88 mM. ^c 1.29 mM [Cp₂Co][S₃N₃]. ^d 0.4 M [nBu_4N][PF₆], $\nu = 0.1 - 0.5$ V s^{-1} . ^e 2.21 mM. ^f 2.08 mM [Cp₂Co][S₃N₃]. ^g 1.05 mM. ^h 1.30 mM [Cp₂Co][S₃N₃].

Simulations of CV Responses for S₄N₄ and [S₃N₃][−]. Theoretical cyclic voltammograms were simulated with the DigiElch simulation package (www.elchsoft.com). The simulation algorithm used in this program has been described previously.²³ Values for the ohmic resistance (R_u) were determined by measuring the impedance of the system at potentials where the Faradaic current was negligibly small. Unless otherwise stated, the charge-transfer coefficients were assumed to be 0.5, and the average values for the diffusion coefficients of S₄N₄ and [S₃N₃][−] were taken to be $1.17 \times 10^{-5} \text{ cm}^2 \text{ s}^{-1}$ and $4.00 \times 10^{-6} \text{ cm}^2 \text{ s}^{-1}$, respectively.

Bulk Electrolysis and ex situ EPR Experiments. Bulk electrolysis was performed by using a cylindrical platinum electrode, a planar platinum mesh auxiliary electrode, and a silver wire quasi-reference electrode, both separated from the solution by 1.0–1.6 μm porosity frits, in a previously described cell.²⁴ Ex situ EPR experiments were conducted on a solution of [Cp₂Co][S₃N₃] in CH₂Cl₂ at 0°C. Oxidative electrolysis at −0.2 V (vs. Fc/Fc⁺) was commenced and after approximately one minute, a one mL aliquot of the oxidized solution was taken and injected into a 4mm (o.d.) quartz EPR tube which had been previously vacuum purged and backfilled with N_{2(g)}. The tube was immediately capped and inserted into liquid nitrogen. This procedure was repeated three more times at one minute intervals, and the four samples were taken and inserted into the EPR cavity held at −153 °C.

SEPR Experiments. SEPR experiments were conducted on solutions of S₄N₄, [Cp₂Co][S₃N₃], and [PPN][S₃N₃] in CH₂Cl₂/[ⁿBu₄N][PF₆] at temperatures between −80 and +30 °C, as well on 99% ¹⁵N-enriched and 99.92% enriched ³³S labeled S₄N₄. The room temperature studies were conducted with a Wilmad quartz electrolytic flat cell with a laminated gold-micromesh working electrode described previously.¹² Low-temperature studies employed a miniature quartz flat cell (Wilmad WG-808) incorporating modified electrodes which are all fed

in from the top of the cell which therefore fits inside the standard Bruker N₂ Dewar insert. The Bruker EMX 113 spectrometer was operated at X-band frequencies (9.8 GHz) and spectra were monitored in intensity-versus-field mode during electrolysis as well as in intensity-versus-time mode after electrolysis was terminated. Plots of $\ln(C_t/C_{t=0})$ vs t (where C = signal intensity, t = time in seconds) as well as of $1/(C_t/C_{t=0})$ vs t were used to determine the rate of decay of the radicals. Simulations of EPR spectra were performed with Bruker Simfonia (version 1.25) and WinSim (version 0.98, 2002) software.²⁵ Experimental g -values were determined with reference to external, solid DPPH (2.0037 ± 0.0002).²⁶ Spectral parameters for [S₄N₄]^{•−} in CH₂Cl₂: conversion times (CT) = 40.96 or 81.92 s, sweep width (SW) = 6.0 mT, modulation amplitude (MA) = 0.05 mT; for ¹⁵N labeled [S₄N₄]^{•−} in CH₂Cl₂: CT = 40.96 or 81.92 s, SW = 6.0 mT, MA = 0.05 mT; for ³³S labeled [S₄N₄]^{•−} in CH₂Cl₂: CT = 40.96 or 81.92 s, SW = 12.0 mT, MA = 0.1 mT. The temperature inside the EPR cavity was calibrated using a Copper-Constantan Thermocouple which was previously calibrated using both ice/water and dry ice/CH₃OH baths. The temperatures were recorded at ten degree intervals against the VT controller over the range of −89 to +19.5 °C.

Crystallography. A small block of [PPN][S₃N₃] cut from a longer pale-green needle was mounted on a glass capillary using Paratone™ oil and cooled to −173(2)°C. The ambiguous space group choice between Cc and $C2/c$ was investigated by solving the structure in both space groups. Full details are provided in the ESI as well as in the electronic CIF file.²⁷ These data can be obtained free of charge from the Cambridge Crystallographic Data Centre via www.ccdc.cam.ac.uk/products/csd/request/request.php4.

Computational Details. Theoretical calculations were carried out for the [S₃N₃][•] radical using Hartree-Fock (HF), Möller-Plesset perturbation theory (MP2),²⁸ coupled cluster (CCSD)²⁹

and complete active space (CAS) methods,³⁰ Dunning's correlation consistent basis set of triple-zeta quality, cc-pVTZ, was used for all atoms.³¹ The CAS calculations utilized a minimum active space consisting of three orbitals and three electrons *i.e* [3,3]-CAS. Harmonic vibrational frequencies were calculated for all optimized geometries. Software used included Gaussian 03,³² Molpro 2002.6³³ and gOpenMol.³⁴

Results and Discussion

Characterization of [PPN][S₃N₃·HOCH₃]. Of the known salts of [S₃N₃][−]^{4,16,17,35} there are five reported crystal structures, for which the cations are [*n*-Bu₄N],^{4g} [(PhCN₂S₂)₂Cl],³⁵ [PhCN₂S₂],^{16a} [PPh₄],^{4f} and [CoCp₂]¹⁷. Here we report the structure of [PPN][S₃N₃] obtained on lime-green crystals from CH₂Cl₂/CH₃OH.³⁶ The anion and solvent are shown in Figure 1, and the asymmetric unit including [PPN]⁺ is provided in the ESI as Figure S1. Selected bond lengths and angles for this compound are listed in Table 2. The average S–N bond lengths and angles from the five previously reported salts are: S–N = 1.607(21) Å; ∠SNS = 123.8(10)°; ∠NSN = 116.1(9)° (all data were collected at 22 °C). The S–N distances and angles are not significantly different in [PPN][S₃N₃] due to the wide range observed in known structures. [S₃N₃][−] is found to be almost planar in the crystal lattice (mean rms deviation below 2.6%, less than observed for any of the six phenyl rings in the cation) but the bond distances and angles do appear distorted as a consequence of the H-bonding interaction with the methanol solvate molecule, with the longest bond and angle adjacent to H. However, the large published variation in these parameters in previous structures leaves this assignment inconclusive. The H-bond between MeOH and the N(2) nitrogen atom is quite typical with a length of 2.829 Å and a bond angle of 162.3°.

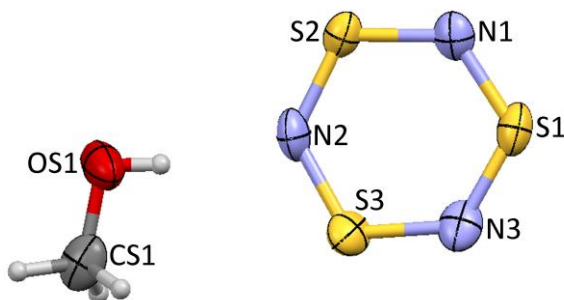


Figure 1. A thermal ellipsoid plot (Mercury 2.2, CCDC, 2008) showing the anion and hydrogen-bonded CH₃OH molecule as determined in the crystal structure of [PPN][S₃N₃·HOCH₃].

Table 2. Selected Bond Lengths [Å] and Angles [°] for [PPN][S₃N₃·HOCH₃].

N(1)-S(1)	1.615(5)	S(1)-N(1)-S(2)	123.8(3)
N(1)-S(2)	1.630(5)	S(2)-N(2)-S(3)	124.2(3)
N(2)-S(2)	1.616(6)	S(1)-N(3)-S(3)	123.2(4)
N(2)-S(3)	1.646(5)	N(3)-S(1)-N(1)	117.5(3)
N(3)-S(1)	1.605(6)	N(2)-S(2)-N(1)	115.4(3)
N(3)-S(3)	1.632(6)	N(3)-S(3)-N(2)	115.5(3)
N(4)-P(2)	1.577(4)	P(2)-N(4)-P(1)	136.1(2)
N(4)-P(1)	1.593(4)	N(4)-P(1)-C(1)	111.4(2)

Voltammetry. S₄N₄, [Cp₂Co][S₃N₃], and [PPN][S₃N₃] were studied by CV in CH₂Cl₂ over scan rates of 0.05–20 V s⁻¹ and temperatures of 21 ± 2 °C. Voltammetric results for S₄N₄, [Cp₂Co][S₃N₃], and [PPN][S₃N₃] in CH₂Cl₂ are reported in Table 3. Representative CVs obtained from solutions of S₄N₄ at a scan rate of 0.2 V s⁻¹ are shown in Figure 2. CVs of the initial reduction process of S₄N₄ within a narrow potential window displayed a small return wave at moderate-to-slow scan rates, which increased in peak current height with increasing scan rate. A close-to-linear scaling of the Faradaic current was observed with concentration of S₄N₄ in CH₂Cl₂ (Table S2), implying that the influence of uncompensated resistance was minimal under our high supporting electrolyte (0.4 M [nBu₄N][PF₆]) conditions. Coulometric measurements (*vide infra*) indicate that the overall process involves the transfer of approximately 1.3 electrons

per S_4N_4 molecule; this strongly suggests an initial one-electron reduction process followed by recycling of “NS”. A second, irreversible reduction process occurs at approximately -1.6 V vs Fc/Fc^+ which has not been explored further.

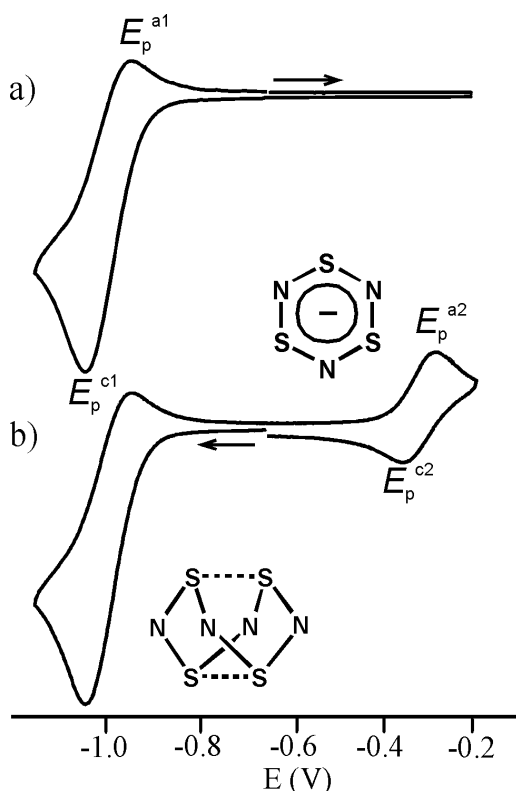


Figure 2. CVs over an extended potential window obtained on 3.90 mM solutions of S_4N_4 in CH_2Cl_2 containing 0.4 M $[nBu_4N][PF_6]$ at a GC electrode at $21.5^\circ C$, $\nu = 0.2$ V s^{-1} with the potential starting at -0.65 V: (a) sweeping in the positive direction and (b) sweeping in the negative direction.

CVs obtained over an electrochemical window that was extended considerably in the anodic direction show the absence (Figure 2a) of secondary processes when the initial sweep direction is anodic, but the presence (Figure 2b) of a new redox couple at $E_n = -0.33$ V vs. Fc/Fc^+ when the potential is first swept through the reduction process. This indicates that the new process involves a species generated from the decomposition of $[S_4N_4]^{\bullet-}$. On the basis of prior investigations (*vide supra*), the new process is attributed to the $[S_3N_3]^{-/0}$ redox couple. Williford *et al.* claimed to have seen several products oxidizable at potentials more positive than the

reduction of S_4N_4 in $CH_3CN/[Et_4N][ClO_4]$ at RT but did not report any details on these processes.^{3c}

Table 3. CV Data obtained for S_4N_4 , $[Cp_2Co][S_3N_3]$, and $[PPN][S_3N_3]$ in CH_2Cl_2 ^a.

compd	conc (mM)	E_p^{a1} (V)	E_p^{c1} (V)	E_m^b (V)	E_p^{a2} (V)	E_p^{c2} (V)	E_n^c (V)
S_4N_4	3.90	−0.93	−1.06	−1.00	−0.29	−0.36	−0.33
$[Cp_2Co][S_3N_3]^d$	2.16		−1.03		−0.30	−0.38	−0.34
$[PPN][S_3N_3]$	3.90	−0.95	−1.04	−1.00	−0.31	−0.37	−0.34

^a Obtained at a GC electrode at $v = 0.2 \text{ V s}^{-1}$ and $T = 21 \pm 1 \text{ }^\circ\text{C}$.

^b $E_m = [E_p^{a1} + E_p^{c1}]/2 \approx E^{o/(1)}$.

^c $E_n = [E_p^{a2} + E_p^{c2}]/2 \approx E^{o/(2)}$.

^d $E^{o/(3)} = [E_p^{a3} + E_p^{c3}]/2 = -1.35 \text{ V}$, ($E_p^{a3} - E_p^{c3} = 100 \text{ mV}$).

We have therefore investigated both $[PPN][S_3N_3]$ and $[Cp_2Co][S_3N_3]$ by CV under identical conditions to those employed for solutions of S_4N_4 . CVs of $[PPN][S_3N_3]$ in CH_2Cl_2 clearly show $[S_3N_3]^{-/0}$ at $E_n = -0.34 \text{ V}$ vs. Fc/Fc^+ ³⁷ but the absence of any further redox couples up to the solvent limit when the scan is first swept in the cathodic direction. Once the potential is swept anodically over potentials including the $[S_3N_3]^{-/0}$ redox couple and the sweep direction is reversed, a new redox couple appears at -1.00 V . CVs of $[Cp_2Co][S_3N_3]$ in CH_2Cl_2 also show the $[S_3N_3]^{-/0}$ redox couple at $E_n = -0.34 \text{ V}$, and another couple at $E^{o/} = -1.35 \text{ V}$, attributable to $[Cp_2Co]^{0/+}$, with a shoulder at -1.03 V (Figure 3). The appearance of these secondary features with comparable E_p^{c1} values to those of S_4N_4 subsequent to cycling the potentials through $[S_3N_3]^{-/0}$ indicates rapid generation of S_4N_4 , presumably from decay of neutral $[S_3N_3]^*$. A third reduction process occurs at ca. -2.30 V in $[Cp_2Co][S_3N_3]$, which is readily attributed to the $[Cp_2Co]^{-/0}$ redox couple.²⁰ A second, irreversible oxidation peak is also seen at $+0.72 \text{ V}$ which has a much smaller peak current height when compared to $[S_3N_3]^{-/0}$. No other redox couples appeared within the solvent window (-2.3 to $+1.6 \text{ V}$).

The $[\text{S}_3\text{N}_3]^{-/0}$ redox couple displayed sizable return waves at moderate scan rates ($0.1 - 0.5 \text{ V s}^{-1}$) and temperatures of $22 \pm 2 \text{ }^\circ\text{C}$, with I_p^{c2}/I_p^{a2} values between $0.62 - 0.69$ which are similar to those observed from $[\text{S}_3\text{N}_3]^-$ generated from bulk S_4N_4 solution (Figure 2). However, the peak currents of the $[\text{S}_3\text{N}_3]^{-/0}$ and $[\text{Cp}_2\text{Co}]^{0/+}$ processes were consistently observed to be uneven ($I_p^{a2}/I_p^{c3} \sim 0.56 - 0.57$), despite the fact that the two species were present in identical concentration in view of their common source in one salt (Figure 3).

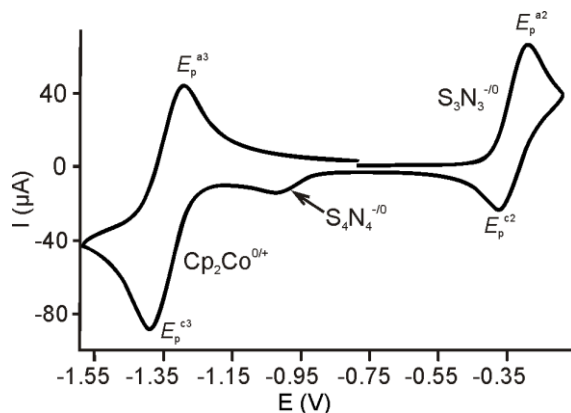


Figure 3. CV obtained on 2.16 mM solutions of $[\text{Cp}_2\text{Co}][\text{S}_3\text{N}_3]$ in CH_2Cl_2 at a GC electrode at $22 \text{ }^\circ\text{C}$, $0.4 \text{ M } [\text{nBu}_4\text{N}][\text{PF}_6]$, $v = 0.2 \text{ V s}^{-1}$.

The peak current of a CV wave under Nernstian conditions is given by Eqn. 1.²¹ Thus, $I_p \propto \sqrt{D_0}$ and estimates for the diffusion coefficient of $[\text{Cp}_2\text{Co}]^+$ ions are $1.66 \times 10^{-5} \text{ cm}^2 \text{ s}^{-1}$ in $\text{CH}_2\text{Cl}_2/[\text{nBu}_4\text{N}][\text{PF}_6]$ ³⁸ and $1.7 \times 10^{-5} \text{ cm}^2 \text{ s}^{-1}$ in CH_2Cl_2 alone (by NMR methods).³⁹ The use of these values and the average diffusion coefficient of $[\text{S}_3\text{N}_3]^-$ from this study (see Table 1) predicts a current ratio of ca. 0.49, which is in reasonable agreement with that observed in the CVs. Hence, we attribute the unusually small peak currents for the oxidation of $[\text{S}_3\text{N}_3]^-$ to the anomalously small diffusion coefficient of this ion in CH_2Cl_2 . A close-to-linear scaling of the Faradaic current was observed with concentration of $[\text{S}_3\text{N}_3]^-$ in CH_2Cl_2 (Table S3), implying that the influence of uncompensated resistance was minimal at this concentration of supporting electrolyte ($0.4 \text{ M } [\text{nBu}_4\text{N}][\text{PF}_6]$).

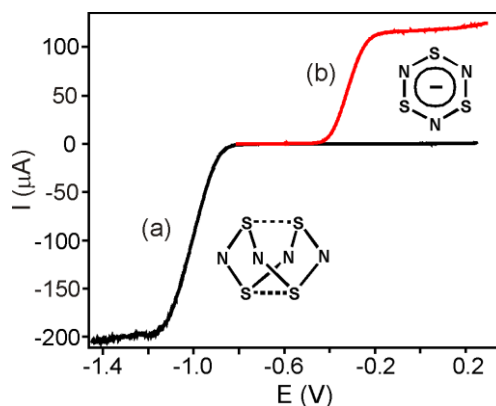


Figure 4. RDE voltammograms obtained on a 1.29 mM solution of S_4N_4 at a 5 mm GC electrode rotating at 500 RPM, $\nu = 0.01 \text{ V s}^{-1}$ at 0°C , showing (a) potential sweep from + 0.25 V to -1.45 V (—) before electrolysis, and (b) potential sweep from -0.9 V to +0.25 V after exhaustive electrolysis at -1.25 V (—).

Bulk Electrolysis of S_4N_4 . The conversion of S_4N_4 to $[\text{S}_3\text{N}_3]^-$ has been claimed to be almost quantitative via exhaustive electrolysis of S_4N_4 at potentials corresponding to the first reduction process in both CH_3CN ^{3e} and anhydrous ethanol.^{4a,b} We undertook to check the validity of such a conversion in CH_2Cl_2 , the solvent used in this study, and have monitored the electrolysis both by coulometry and by RDE voltammograms taken before and after the completion of electrolysis (Figure 4). Electrolysis of 1.29 mM solutions of S_4N_4 in $\text{CH}_2\text{Cl}_2/(0.1 \text{ M } [\text{nBu}_4\text{N}][\text{PF}_6])$ at -1.25 V (vs. Fc/Fc^+) for 41 minutes led to the disappearance of the wave for S_4N_4 , and the growth of a new wave corresponding to the half-wave potential for oxidation of $[\text{S}_3\text{N}_3]^-$. Quantitative conversion is indicated both by the value of n , the number of electrons transferred (1.3 per S_4N_4), from coulometry and the size of the RDE currents. The much larger current for S_4N_4 (at $\frac{3}{4}$ the concentration of $[\text{S}_3\text{N}_3]^-$) should be placed in the context of the large difference in diffusion coefficients for the two species. Using the ratio of the 200 and 118 μA limiting currents to the average D_0 values and the 4:3 stoichiometry ratio, the RDE voltammograms indicate essentially complete conversion (~97%), in good agreement with the value from coulometry.

SEEPR Experiments: EPR Spectra of $[\text{S}_4\text{N}_4]^-$. Utilization of a conventional aqueous flat cell with a very large surface-area working electrode allowed observation of a nine-line spectrum (Figure S2) after single 82 s scans at RT. This spectrum was recognizably the same as that reported previously at temperatures below 0 °C,^{3b,c} but with excessively broadened lines (line width, LW, = 0.135 mT, $a(\text{N}) = 0.117$ mT). By switching to a smaller low-temperature SEEPR cell, high quality EPR spectra from single 41 s or 82 s scans were obtained upon reductive electrolysis at -1.10 V at 0 °C or lower (Figures 5,6). With natural-abundance S_4N_4 , the expected nine-line pattern is readily simulated using four equivalent $a(^{14}\text{N}) = 0.1175$ mT, LW = 0.06 mT, and g value = 2.0008(1), in good agreement with the literature values (Table 4).^{3b,c} Spectra obtained at temperatures between -80 to 0 °C are of similar quality with little apparent variation in LW, while those collected above 0 °C suffer from line-broadening similar to that observed at room temperature.

Table 4. Experimental and Calculated EPR Data for $[\text{S}_4\text{N}_4]^-$.

nucleus	expt hfs (mT)	calc hfs (mT) ¹⁴	line width (mT)	g value	solvent
$^{14}\text{N}_{1-4}$ ^a	0.1185(1) ^{3b}	0.08	0.046	2.0006(1)	THF
$^{14}\text{N}_{1-4}$ ^b	0.117(2) ^{3c}	0.08	0.05	not reported	CH_3CN
$^{14}\text{N}_{1-4}$ ^b	0.1175	0.08	0.06	2.0008(1)	CH_2Cl_2
$^{15}\text{N}_{1-4}$ ^c	0.1635	—	0.05	2.0008(1)	CH_2Cl_2
$^{33}\text{S}_{1,2}$ ^d	0.2	-0.65^{39}	0.08	2.0008(1)	CH_2Cl_2
$^{33}\text{S}_{3,4}$ ^d	0.2	0.97^{39}	0.08	2.0008(1)	CH_2Cl_2

^a $[\text{}^n\text{Bu}_4\text{N}][\text{ClO}_4]$ as the supporting electrolyte, -25 °C.

^b $[\text{Et}_4\text{N}][\text{ClO}_4]$ as the supporting electrolyte, -20 °C.

^c 1.2 mM solution with 0.4 M $[\text{}^n\text{Bu}_4\text{N}][\text{PF}_6]$ as the supporting electrolyte, -10 °C.

^d 5.4 mM solution with 0.4 M $[\text{}^n\text{Bu}_4\text{N}][\text{PF}_6]$ as the supporting electrolyte, -20 °C.

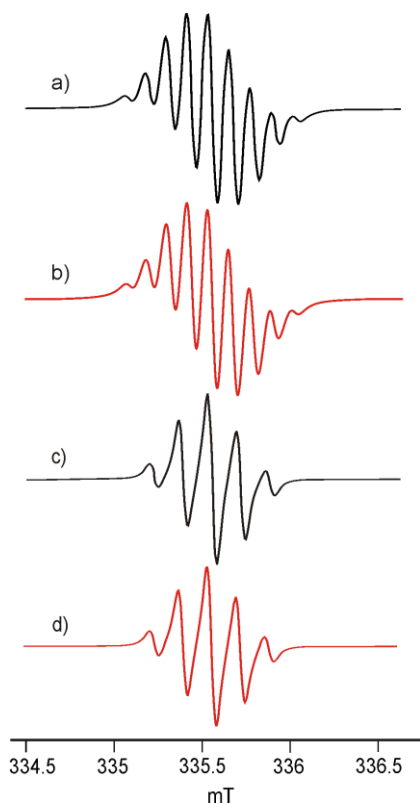


Figure 5. (a) Experimental (—) and (b) simulated (—) first derivative EPR spectra obtained during in situ reductive electrolysis (82 s single scan) of a 3.1 mM solution S_4N_4 at a gold micromesh electrode at $-20\text{ }^{\circ}\text{C}$ in CH_2Cl_2 (0.4 M $[^nBu_4N][PF_6]$): modulation amplitude = 0.05 mT. (c) Experimental (—) and (d) simulated (—) spectra obtained in similar manner from a 1.2 mM solution of 99 % enriched $^{32}S_4^{15}N_4$ at a gold micromesh electrode at $-10\text{ }^{\circ}\text{C}$ in CH_2Cl_2 (0.4 M $[^nBu_4N][PF_6]$): modulation amplitude = 0.05 mT. g value = 2.0008(1).

SEPR studies of 99% ^{15}N isotope-enriched $^{32}S_4^{15}N_4$ were performed in CH_2Cl_2 over the same temperature range. An example of a typical spectrum observed from one 82 s scan at -10°C is shown in Figure 5c. The characteristic five-line pattern with $a = 0.1635\text{ mT}$, $LW = 0.05\text{ mT}$, and intensity ratio 1:4:6:4:1 is consistent with coupling to four equivalent ($I = \frac{1}{2}$) ^{15}N nuclei. The ratio of $a(^{14}N)/a(^{15}N)$ fits well to the gyromagnetic ratio's. In the same way, SEPR studies were attempted on 99.92% ^{33}S -enriched $^{33}S_4^{14}N_4$. The resulting very broad, low-intensity signal (Figure 6a) was difficult to detect and the sample was subsequently spiked with some natural abundance material. The experimental spectra resulting from reductive electrolysis on samples containing this mixture were easier to detect, facilitating the collection of data with adequate

signal-to-noise ratio (Figure 6b). Subtraction of the $[\text{}^{32}\text{S}_4\text{}^{14}\text{N}_4]^\bullet$ component from the signal followed by digital filtering afforded a broad, undistorted singlet due solely to $[\text{}^{33}\text{S}_4\text{}^{14}\text{N}_4]^\bullet$ (Figure 6c). A reasonable simulation of this signal is obtained (Figure 6d) by employing the values for $a(^{14}\text{N}_{1-4}) = 0.12$ mT and $\text{LW} = 0.08$ mT determined for the $[\text{}^{32}\text{S}_4\text{}^{14}\text{N}_4]^\bullet$ component before subtraction, and fitting the lineshape by including additional coupling from four equivalent S nuclei with $a(^{33}\text{S}_{1-4}) = 0.20$ mT. Simulations using two pairs of inequivalent values for $a(^{33}\text{S})$ gave a poorer fit. The DFT (UB3LYP/aug-cc-pVTZ) calculated hfs constants for the static C_{2v} minimum structure of $[\text{S}_4\text{N}_4]^\bullet$ from our previous report¹⁴ are $a(^{33}\text{S}_{1,2}) = -0.65$ and $a(^{33}\text{S}_{3,4}) = 0.97$ mT.⁴⁰ Exchange can result in averaging of the hfs constants of the interchanged nuclei as seen for example in the cyclopentadienyl radical;⁴¹ magnetic interactions between the ^{14}N and ^{33}S nuclei can also lead to more than simple averaging of the couplings such as occurs in the EPR spectrum of dinitrodurene at elevated temperatures.⁴² Support for the notion of a rapid conformational equilibrium in $[\text{S}_4\text{N}_4]^\bullet$ at -20 °C is provided by considering the average of the calculated ^{33}S hfs constants for the two kinds of sulfur nuclei which, at 0.16 mT, is in very good agreement with the ~ 0.2 mT obtained from the simulation. Note that in the specific case of $[\text{S}_4\text{N}_4]^\bullet$, lower levels of ^{33}S doping *do not* lead to more easily interpretable EPR spectra.

EPR Investigations of $[\text{S}_3\text{N}_3]^\bullet$. Our previously reported calculations indicate that $[\text{S}_3\text{N}_3]^\bullet$ should possess a planar ring structure (cf. $[\text{S}_3\text{N}_3]^-$), which is mildly distorted towards C_{2v} symmetry as a result of a Jahn-Teller effect.¹⁴ This distortion is reflected in the calculated hfs constants, with two different ^{14}N ($a(\text{N})_{1,2} = 0.57$ mT, $a(\text{N})_3 = -0.18$ mT) and ^{33}S ($a(\text{S})_{1,2} = 0.60$ mT, $a(\text{S})_3 = 0.11$ mT) values. The predicted EPR spectrum based on the calculated isotropic hfs constants with natural abundances of the isotopes is shown in Figure S3(a), along with the high-symmetry spectrum that might result from dynamic exchange with (weighted) average hfs

constants ($a(\text{N})_{1-3} = 0.32$ mT, Figure S3(b)). There is every reason to have confidence in hfs constants calculated at this level of theory for planar S,N ring compounds.¹⁴

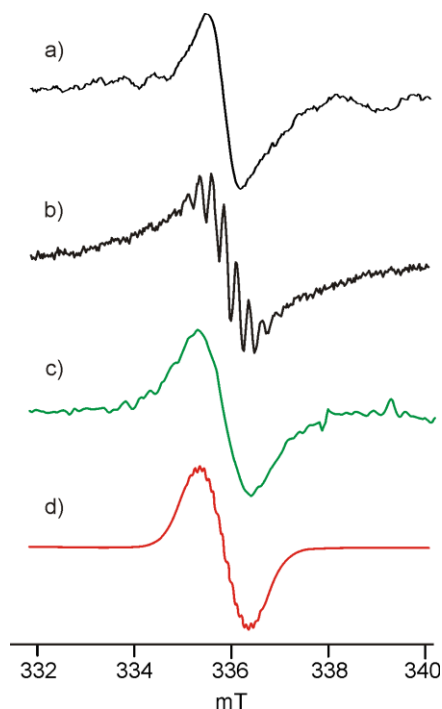


Figure 6. (a) Experimental EPR spectrum of $[\text{}^{33}\text{S}_4\text{}^{14}\text{N}_4]^{-\bullet}$ at -20 °C after strong digital filtering (—), (b) experimental EPR spectrum of $[\text{}^{33}\text{S}_4\text{}^{14}\text{N}_4]^{-\bullet}$ spiked with $[\text{}^{32}\text{S}_4\text{}^{14}\text{N}_4]^{-\bullet}$ at -20 °C (—), (c) spectrum of $[\text{}^{33}\text{S}_4\text{}^{14}\text{N}_4]^{-\bullet}$ after subtraction of the spike and moderate digital filtering (—), and (d) simulation (—), with $a(^{33}\text{S}_{1-4}) = 0.2$ mT, $a(^{14}\text{N}_{1-4}) = 0.12$ mT. g value = 2.0008(1).

Our attempts to observe this radical in condensed phases began with low temperature SEEPR studies of CH_2Cl_2 solutions containing either $[\text{Cp}_2\text{Co}][\text{S}_3\text{N}_3]$ or $[\text{PPN}][\text{S}_3\text{N}_3]$. Oxidative electrolysis at a potential of -0.2 V at temperatures between -60 and $+20$ °C did not generate a spectrum that could be conclusively attributed to $[\text{S}_3\text{N}_3]^\bullet$. A persistent five-line pattern was observed (Figure 7), which did not increase in intensity with electrolysis at -0.2 V or decay after stopping electrolysis. The signal did seem to be induced by the presence of the electrodes in solution, and to grow in intensity at lower temperatures. The spectra displayed significant line width variation over the 120 °C temperature range and have a g value of 2.0105. While they could be simulated by using two equivalent nitrogen hfs constants of 0.509 mT, and one

(unresolved) nitrogen hfs constant of 0.044 mT, these values do not agree with the calculated hfs as discussed above. Furthermore, the persistent nature of this EPR signal is inconsistent with the estimated lifetime of $[\text{S}_3\text{N}_3]^{\bullet}$ (*vide infra*). We did confirm, however, that $[\text{S}_3\text{N}_3]^{-}$ is oxidized to S_4N_4 during these experiments by generation of the nine-line spectrum of $[\text{S}_4\text{N}_4]^{\bullet-}$ upon subsequent switching to electrolysis at -1.1 V (Figure 7).

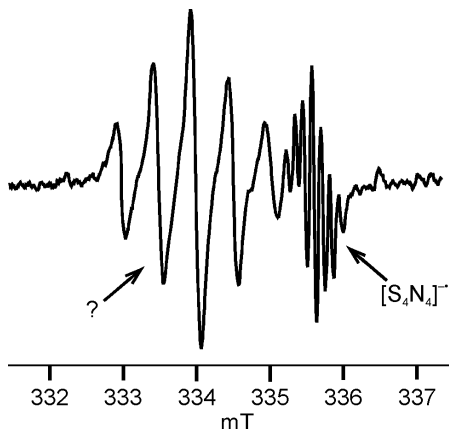


Figure 7. Experimental first derivative EPR spectra obtained during in situ reductive electrolysis of $[\text{PPN}][\text{S}_3\text{N}_3]$ at -1.1 V (82 s single scan) following initial electrolysis at -0.2 V at a gold mesh electrode at -60 °C in CH_2Cl_2 (0.4 M $[\text{tBu}_4\text{N}][\text{PF}_6]$), modulation amplitude = 0.2 mT. g values = 2.0105 (left signal), 2.0008 (right signal).

Note that the persistence of the five-line pattern during electrolysis at such negative potentials is also inconsistent with the postulate that it is due to $[\text{S}_3\text{N}_3]^{\bullet}$. Similar five-line spectra have been seen previously and were assigned to the presence of $[\text{NSN}]^{\bullet-}$, a common decomposition product of many unstable S,N species.^{3a,43} This species is reported to possess equivalent ^{14}N nuclei with $a(\text{N}) \sim 0.50\text{--}0.52$ mT and to have g values in the range 2.0105(5) to 2.0103, which fits well with the signal we observe. The line width dependence that we observed for this signal, apparently for the first time, would also seem to be more consistent with a bent σ radical than with a planar S_3N_3 π -radical. We do not know how the species causing this signal arises but the following observations can be made: (i) this EPR signal is never seen during electrolysis of pure S_4N_4 solutions; (ii) it does not increase in intensity in response to electrolysis

over the potential range 0 to -1.3 V. Though $[\text{NSN}]^{\bullet-}$ could arise from disproportionation of $\text{S}_3\text{N}_3^{\bullet}$ (along with the known $[\text{SNS}]^+$ ion),¹⁴ this cannot be the dominant decomposition pathway in view of observation (ii).

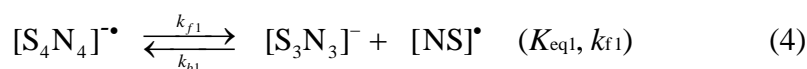
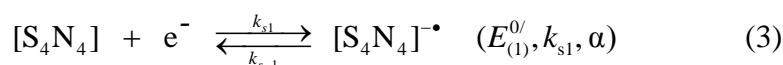
As an alternative route to $[\text{S}_3\text{N}_3]^{\bullet}$, we carried out bulk reductive electrolysis of S_4N_4 in CH_2Cl_2 at -1.25 V, followed by transfer of the newly generated $[\text{tBu}_4\text{N}][\text{S}_3\text{N}_3]$ solution to the SEEPR cell, and then performing in situ oxidative electrolysis of $[\text{S}_3\text{N}_3]^-$. This led to results very similar to those found when using $[\text{Cp}_2\text{Co}][\text{S}_3\text{N}_3]$ and $[\text{PPN}][\text{S}_3\text{N}_3]$ for such experiments. The bulk oxidative electrolysis of a CH_2Cl_2 solution containing $[\text{Cp}_2\text{Co}][\text{S}_3\text{N}_3]$ at -0.2 V was also attempted. Aliquots of the oxidized solution were syringed out at one minute intervals into EPR tubes and frozen in LN_2 and inserted into the EPR cavity. No notable EPR signals were detected from any of the frozen aliquots collected. All attempts to detect $[\text{S}_3\text{N}_3]^{\bullet}$ have thus far been unsuccessful, corroborating earlier failures reported by other workers.^{10,16}

EPR Lifetime Measurements. Rate constants from the decay of the EPR signal of $[\text{S}_4\text{N}_4]^{\bullet-}$ in CH_2Cl_2 at temperatures between -88.4 and $+25.6$ °C and concentrations of 2 and 5 mM were determined by generating the radical electrochemically, halting electrolysis and measuring the decay of the signal intensity as a function of time at constant field. The slope of the plots of $\ln(C_t/C_{t=0})$ vs t (C = signal intensity) yielded k_{f1} values in the range of $0.0052 - 1.85$ s⁻¹ over a 70°C temperature range (Table S4). Plots that were based on second-order kinetics exhibited a much poorer fit to the data, consistent with a previous report.^{3c} The accuracy of k_{f1} values was found to be negatively affected at lower temperatures by a competing factor, the diffusion of the radical anion out of the EPR cavity more rapidly than its actual decay (see ESI, Figures S4, S5). Therefore only rate constants between the temperatures of -22 and $+16$ °C were used in an Arrhenius activation energy plot (Figure S6); which yielded a value of 62 ± 2 kJ/mol. This value

is slightly higher than the literature value of 47 ± 4 kJ/mol,^{3c} which may be due to the different solvent used in our study, but also may suggest that the statistical uncertainty in such measurements significantly underestimates the true errors.

Simulations of the Cyclic Voltammetric Responses for S₄N₄ and [S₃N₃][−]. Full digital simulations of the CV responses were carried out in order to obtain kinetic data for the [S₄N₄]^{−/0} and [S₃N₃]^{−/0} redox couples in solutions of S₄N₄, [Cp₂Co][S₃N₃] and [PPN][S₃N₃]. All simulations employed independently measured values for the electrode area, analyte concentration, temperature, diffusion coefficient D , and uncompensated solution resistance R_u . Values for D (Table 1) for both S₄N₄ and [S₃N₃][−] were obtained from RDE voltammetry experiments, and were assumed to be equivalent for the corresponding oxidized or reduced counterparts.

[S₄N₄]^{−/0}. Digital simulations of CVs obtained for the [S₄N₄]^{−/0} redox couple over a range of scan rates $\nu = 0.1 - 0.5$ V s^{−1} at two concentrations were performed in order to quantify the decay of the reduction product as described by an EC mechanism:⁴⁴

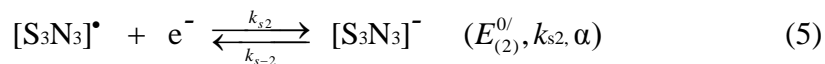


where k_s and α are, respectively, the standard heterogeneous rate constant and the transfer coefficient associated with the Butler-Volmer formalism²¹ for a heterogeneous electron transfer; K_{eq1} and k_{f1} are the equilibrium constant and the rate constant for the follow-up chemical reaction. The first-order nature of the decay of [S₄N₄]^{−•} was previously established in the more polar solvent CH₃CN,^{3c} and values for k_{f1} at approximately the same temperature obtained in that study were used as a starting point for our own investigations. Several second-order decay mechanisms were also considered, and in all cases these failed to reproduce the experimental

CVs over more than one concentration. Many possibilities were also considered for the first-order decay pathway of the radical anion, which is known to lead ultimately to $[\text{S}_3\text{N}_3]^-$. ECC mechanisms⁴⁴ which included an intermediate between $[\text{S}_4\text{N}_4]^{-\bullet}$ and $[\text{S}_3\text{N}_3]^-$ had parameters for the second C step that did not affect the overall fit, so ECC was abandoned from consideration for this redox couple.

For the EC mechanism,⁴⁴ the adjustable parameters were the apparent $E_{(1)}^{0/}$ as measured vs. the silver-wire quasi reference electrode (see Table 3 for $E^{0/}$ values vs $E_{\text{Fc}^{0/+}}^{0/}$), k_{f1} , and k_{s1} . For the purposes of simulation the value of α was assumed to be 0.5. Various values for the equilibrium constant K_{eq1} were investigated, but small values for K_{eq1} did not lead to optimal fits, so this value was arbitrarily fixed at 10^6 , thus rendering the chemical reaction effectively irreversible over the scan rates investigated. The optimization of simulated CV responses using *DigiElch* was deemed successful when the simulated and experimental peak heights and positions overlaid each other (see Figure S7). Values for the rate constants were determined from fitting CV's obtained at two different concentrations measured over the scan rate range $\nu = 0.1\text{--}0.5 \text{ V s}^{-1}$ (see Table S3) and led to estimates of these values as $k_{\text{s1}} = 0.034 \pm 0.004 \text{ s}^{-1}$ and $k_{\text{f1}} = 1.8 \pm 0.2 \text{ s}^{-1}$. Thus, full line-shape digital simulation of the CV's are consistent with a slow rate of electron transfer to S_4N_4 (i.e. charge-transfer irreversibility, confirming the observations of Williford *et al.* from their study in $\text{CH}_3\text{CN}/[\text{Et}_4\text{N}][\text{ClO}_4]$ below 0°C),^{3c} followed by first-order decay of the initially formed $[\text{S}_4\text{N}_4]^{-\bullet}$.

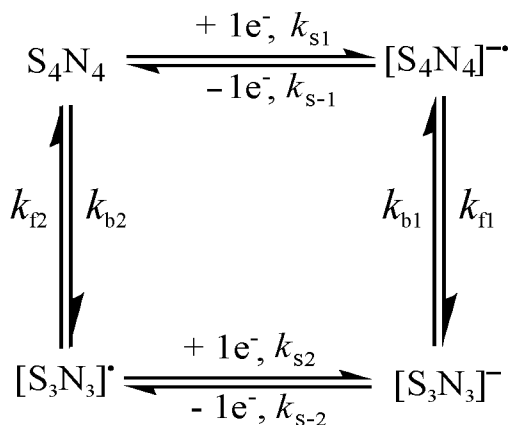
$[\text{S}_3\text{N}_3]^{-/0}$. Digital simulations of CVs obtained for the $[\text{S}_3\text{N}_3]^{-/0}$ redox couple using both $[\text{Cp}_2\text{Co}][\text{S}_3\text{N}_3]$ and $[\text{PPN}][\text{S}_3\text{N}_3]$ as sources of the anion were undertaken using a similar regime to that employed in the previous section, and focused on quantifying the decay of the oxidation product as described by the EC mechanism:⁴⁴



where k_s , α , K_{eq} , and k_f have the same meanings as described previously. Exclusion of any coupled homogeneous chemical steps subsequent to the initial electron transfer failed to accurately reproduce the CVs, consistent with previous evidence for the conversion of $[\text{S}_3\text{N}_3]^{-}$ to S_4N_4 following oxidative electrolysis.¹⁰ Anomalous deviations in the peak current heights led to complications in simulating the CVs, and could be traced to a hypersensitivity of the anion towards oxygen (see ESI for details on how this was overcome). CVs obtained under a rigorous exclusion of oxygen were simulated to determine values for the electron transfer k_{s2} and the decay step k_{f2} rate constants. Both first- and second-order decay mechanisms were considered. Those which considered the radical to react with itself (dimerization) or with $[\text{S}_3\text{N}_3]^{-}$ failed to reproduce the CVs. For the EC mechanism described above, the adjustable parameters were the apparent $E_{(2)}^{0/}$ (see Table 4 for $E^{0/}$ values vs $E_{\text{Fc}^{0/+}}^{0/}$), k_{f2} , and k_{s2} . The value of α was assumed to be 0.5. Various values for the equilibrium constant $K_{\text{eq}2}$ were investigated, but small values for $K_{\text{eq}2}$ did not lead to optimal fits, and thus this value was again arbitrarily fixed at 10^6 . This resulted in good overlap of the simulated and experimental peak heights and positions (Figures S9, S10). Final values for k_{s2} and k_{f2} were determined from fitting CV's obtained at two different concentrations measured over the scan rate range $\nu = 0.1\text{--}0.5 \text{ V s}^{-1}$ (see Table S6) giving estimates of these values of $k_{s2} = 0.022 \pm 0.005 \text{ s}^{-1}$ and $k_{f2} = 0.4 \pm 0.1 \text{ s}^{-1}$. Thus there is also a slow rate of electron transfer for the oxidation of $[\text{S}_3\text{N}_3]^{-}$, followed by an apparent first-order chemical decomposition of the electrogenerated species, which we presume to be the elusive neutral radical $[\text{S}_3\text{N}_3]^{\bullet}$.

$[\text{S}_4\text{N}_4]^{-/0} - [\text{S}_3\text{N}_3]^{-/0}$ **interconversion with first-order decay.** Building on the successful simulations of the individual redox couples we set out to characterize the interconversion of the two electroactive species. While the interconversion is necessarily complex because of the 4:3 stoichiometry (as confirmed by bulk electrolysis), our attempts to incorporate this into the kinetic model were not successful. In the end we applied a simplified "square scheme" mechanism,⁴⁵ depicted in Scheme 1, which simply combines the parameters developed above for the two redox couples independently. We start by simulating CV's obtained on solutions containing bulk S_4N_4 over a larger potential window (-0.2 to -1.15 V, Figure 8). In the full-cycle simulations, the adjustable parameters were $E^o_{(1)}$, $E^o_{(2)}$, k_{f1} , and k_{f2} . The value of α was again assumed to be 0.5. Including k_{s1} and k_{s2} as adjustable parameters resulted in only minor variations in their values (within standard deviation error limits), and therefore these were kept fixed to the average values determined previously ($k_{s1} = 0.03$, $k_{s2} = 0.02$) in order to limit the number of adjustable parameters. K_{eq1} was also kept fixed at 10^6 as before, but in the square scheme this makes K_{eq2} a dependent variable and these parameters are reported among the final fits for completeness (see Table 5).⁴⁵

Scheme 1. A simplified "square scheme" mechanism for the interconversion of S_4N_4 and $[\text{S}_3\text{N}_3]^-$ following first-order decay pathways for both chemical steps. The parameters used here are those defined in Eqn. 3-6.



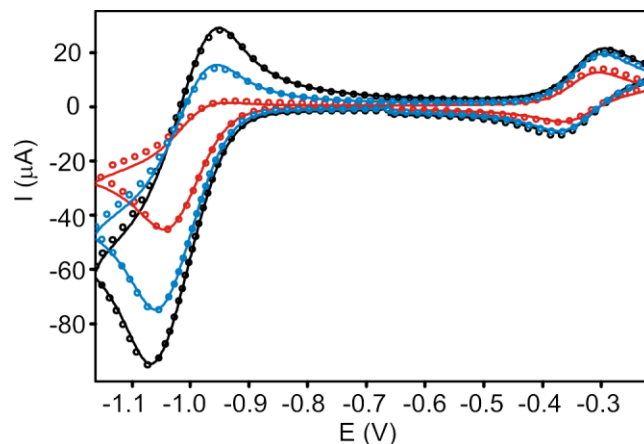


Figure 8. Comparison of the experimental CVs of 2.40 mM S₄N₄ over an extended potential window at 0.1 (—), 0.3 (—), and 0.5 (—) V·s⁻¹ (GC electrode), 0.4 M [tBu₄N][PF₆] in CH₂Cl₂ at 21.1 °C, along with the simulated CVs (0.1 V s⁻¹ = ○○ 0.3 V s⁻¹ = ○○, 0.5 V s⁻¹ = ○○). See Table 9 for simulation parameters.

Table 5. Parameters used in Full Cycle CV Simulations based on Scheme 1 in CH₂Cl₂ on a GC Electrode.^a

bulk compd	conc (mM) ^b	R_u , Ω ^c	$ \Delta E^{o'} $ (V) ^d	k_{f1} (s ⁻¹)	K_{eq1} (×10 ⁶) ^e	k_{f2} (s ⁻¹)	K_{eq2} (×10 ⁵) ^e	T (°C)
S ₄ N ₄	2.40	244	0.67	1.54 ± 0.07	1.00	0.40 ± 0.18	2.5 ± 0.3	21.1
S ₄ N ₄	1.20	222.5	0.66	1.65 ± 0.08	1.00	0.50 ± 0.25	2.0 ± 0.2	23.3
[PPN][S ₃ N ₃]	3.90	242.2	0.65	2.62 ± 1.30	1.00	0.39 ± 0.14	1.5 ± 0.1	21.5
[PPN][S ₃ N ₃]	8.20	238.2	0.65	2.77 ± 0.67	1.00	0.46 ± 0.11	1.7 ± 0.5	19.3
Best est.	—	—	0.66	2.0 ± 0.5	1.00	0.4 ± 0.2	1.9 ± 0.5	21 ± 2

a. Invariant parameters: D (S₄N₄, [S₄N₄]^{-•}) = 1.17 × 10⁻⁵ cm² s⁻¹, D ([S₃N₃]⁻, [S₃N₃][•]) = 4.00 × 10⁻⁶ cm² s⁻¹, as determined by RDE measurements (see Table 1). v = 0.1–0.5 V s⁻¹. k_{s1} = 0.03 (s⁻¹), k_{s2} = 0.02 (s⁻¹), as determined from the average of the values listed in Tables S5 and S6.

b. Invariant parameters determined by original solution composition.

c. R_u values were measured on a PARSTAT 2273 potentiostat.

d. For the experimental potentials vs. Fc see Table 3.

e. K_1 was fixed at a high value after considerable testing of alternatives; K_2 is a dependent variable.

Values for k_{f1} and k_{f2} leading to the best possible overlap of the simulated and experimental peak heights and positions are listed in Table 5; k_{f2} values are in excellent agreement with those determined in the previous [S₃N₃]^{-/0} study and k_{f1} values are just outside the standard deviation determined from the [S₄N₄]^{-/0} study. Choosing to fix the parameters k_{f1} and k_{f2} to the average

values calculated from the previous studies ($k_{f1} = 1.8$, $k_{f2} = 0.4$) showed only minor deviations in the overlap of the simulated versus the experimental peak heights. It is probable that the statistical uncertainty for the k_{f1} values obtained in the $[S_4N_4]^{-/0}$ study underestimates the true errors.

In order to insure the general validity of these parameters, simulations of CV measurements covering a similar extended potential range (-0.15 to -1.1 V) starting from solutions of $[PPN][S_3N_3]$ were also undertaken (Figure 9). The adjustable parameters were again $E^o_{(1)}$, $E^o_{(2)}$, k_{f1} , and k_{f2} . k_{s1} and k_{s2} were again kept fixed at 0.03 and 0.02, respectively, and K_{eq1} was fixed at 10^6 . Once again the k_{f2} values are in excellent agreement with those determined previously, but values for k_{f1} are just outside of the standard deviation from the initial $[S_4N_4]^{-/0}$ study. These results are also compiled in Table 5 and from a conservative comparison of the four data sets from two chemically different species, *best estimates* for the key parameters have been determined as follows: $k_{s1} = 0.034 \pm 0.004$ s⁻¹, $k_{f1} = 2.0 \pm 0.5$ s⁻¹, $k_{s2} = 0.022 \pm 0.005$ s⁻¹ and $k_{f2} = 0.4 \pm 0.2$ s⁻¹. We note that these values using the higher estimated errors are all, within experimental error, the same as those determined for the individual redox couples. Moreover, k_{f1} is in qualitative agreement with rates determined from EPR lifetimes (Table S4). The success of this simple square scheme would then seem to indicate that other processes occurring in solution, such as the elimination of the $[NS]^{\bullet}$ radical from $[S_4N_4]^{\bullet-}$ or the recombination of the former to reform S_4N_4 are not rate-determining.

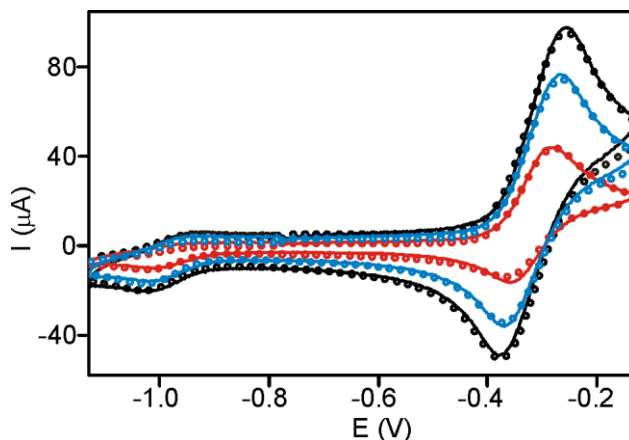


Figure 9. Comparison of the experimental CVs of 3.90 mM [PPN][S₃N₃] over an extended potential window at 0.1 (—), 0.3 (—), and 0.5 (—) V·s⁻¹ (GC electrode), 0.4 M [ⁿBu₄N][PF₆] in CH₂Cl₂ at 21.5 °C, along with the simulated CVs (0.1 V s⁻¹ = ○○, 0.3 V s⁻¹ = ○○, 0.5 V s⁻¹ = ○○). See Table 10 for simulation parameters.

[S₄N₄]⁻⁰ [S₃N₃]⁻⁰ interconversion with involvement of [NS][•]. With a calculated k_{f2} value of 0.4 s⁻¹ for the decay of the oxidation product of [S₃N₃]⁻ ($t_{1/2}$ = 1.7 s at RT), we became even more surprised by our inability to obtain an EPR spectrum of [S₃N₃][•], including measurements taken down to -60 °C, especially given the excellent EPR results for [S₄N₄]^{•-} with its almost 5 times larger k_{f1} value ($t_{1/2}$ = 0.69 s) at RT. So we returned to the simulations of the CV measurements to consider another alternative for the decay of the oxidation product of [S₃N₃]⁻. The alternate pathway that was considered was suggested by careful inspection of concentration profiles generated in *DigiElch* in the simulations starting from bulk S₄N₄ over an extended potential window to include both redox couples (Figure 10). This profile indicates that an approximately 23% [NS][•] concentration is generated at the electrode surface throughout a CV cycle. We postulated that if this quantity of [NS][•] could exist in a solution of S₄N₄, then it was plausible for similar amounts to exist in a solution of [S₃N₃]⁻. Therefore, we assumed an approximately 20% [NS][•] equilibrium concentration in solutions of [PPN][S₃N₃] in the presence of a poised electrode surface which could then react with [S₃N₃][•] to regenerate S₄N₄. This results in a second-order pathway for this step, as described by Scheme 2.

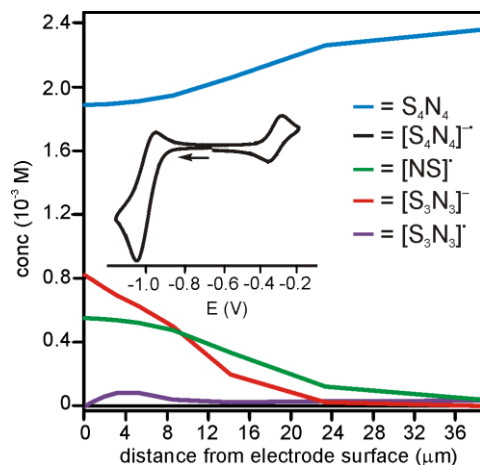
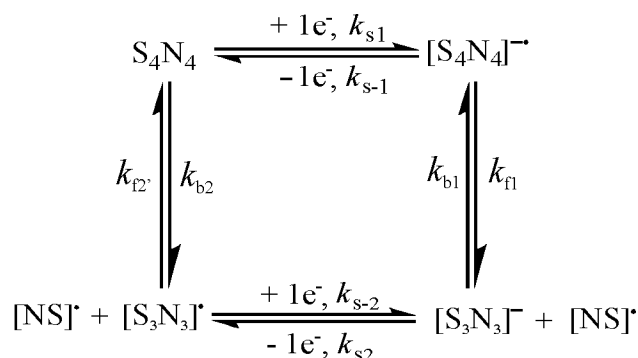


Figure 10. Concentration profile generated from a 2.40 mM S_4N_4 solution and using parameters generated from Scheme 2. The quantity of each species is given subsequent to one complete CV cycle, starting from and ending at -0.7 V, at and beyond the surface of the electrode.

Scheme 2. An alternative "square scheme" mechanism for the involvement of $[NS]^\bullet$ in the interconversion of S_4N_4 and $[S_3N_3]^\bullet$. The second chemical step is now second-order with Rate = $k_{f2}[S_3N_3][NS]$.



The same experimental data were then fitted to the new mechanism. The adjustable parameters for this study were $E^o_{(1)}$, $E^o_{(2)}$, k_{f1} and k_{f2} . Again, k_{s1} and k_{s2} were kept fixed at 0.03 and 0.02, respectively, and again K_{eq1} was fixed at 10^6 , with K_{eq2} as the dependent variable. The fits obtained are comparable to those attained using Scheme 1 and the results are listed in Table 6. However, the fits starting from bulk solutions of $[PPN][S_3N_3]$, unlike S_4N_4 , required the inclusion of an $[NS]^\bullet$ bulk concentration term. These fits resulted in a best estimate for the second-order rate constant k_{f2} of $1.1 \pm 0.3 \times 10^3 \text{ s}^{-1} \text{ M}^{-1}$ and unchanged values for the other parameters. In this case the rate is proportional to the product of two different concentrations for

the second-order reaction (see ESI). Solving for $t_{1/2}'$ results in lifetimes for $[S_3N_3]^\bullet$ in the range of 0.2 to 0.8 s, which are shorter than those estimated from the first-order decay pathway. This may be significant in terms of our inability to detect an EPR signal for this radical. One of the reviewers suggested that dimerization of the radical might still be a factor despite our inability to detect such a process in the voltammetric modeling. A dimer structure has been detected by gas-phase DFT calculations as shown in Figure S11 but the interaction does not appear to be strong. Related sulfur-nitrogen heterocyclic radicals in dilute, cold, solutions are well known to give EPR signals that are easy to detect even though in the solid-state they form dimers. It is certainly the case, however, that dimerization may explain the null results obtained from the frozen solution spectra. Ultimately we still do not have a good explanation for the apparent EPR silence of this free radical.

Table 6. Parameters used in Full Cycle CV Simulations based on Scheme 2 in CH_2Cl_2 on a GC Electrode.^a

Bulk compd ^b	conc [NS] [•] (mM) ^c	$ \Delta E^{o\prime} $ (V) ^d	k_{f1} (s ⁻¹)	K_{eq1} ($\times 10^6$) ^e	k_{f2}' ($\times 10^3$ s ⁻¹ M ⁻¹)	K_{eq2} ($\times 10^5$) ^e	T (°C)
S ₄ N ₄	0	0.67	1.53 ± 0.06	1.00	0.70 ± 0.40	2.6 ± 0.3	21.1
S ₄ N ₄	0	0.67	1.61 ± 0.05	1.00	1.36 ± 0.35	2.2 ± 0.2	23.3
[PPN][S ₃ N ₃]	0.80	0.65	2.79 ± 1.36	1.00	1.25 ± 0.15	1.6 ± 0.1	21.5
[PPN][S ₃ N ₃]	1.60	0.65	2.95 ± 0.67	1.00	1.19 ± 0.49	1.7 ± 0.5	19.3
Best est.	—	0.66	2.2 ± 0.5	1.00	1.1 ± 0.3	2.0 ± 0.3	21 ± 2

a. Invariant parameters: D (S₄N₄, [S₄N₄]^{-•}) = 1.17 × 10⁻⁵ cm² s⁻¹, D ([S₃N₃]⁻, [S₃N₃][•]) = 4.00 × 10⁻⁶ cm² s⁻¹, as determined by RDE measurements (see Table 1). ν = 0.1–0.5 V s⁻¹. k_{s1} = 0.03 (s⁻¹), k_{s2} = 0.02 (s⁻¹), as determined from the average of the values listed in Tables S5 and S6.

b. For the concentration of the bulk compound and R_u values, see Table 5.

c. As determined from the simulations only.

d. For the experimental potentials vs. Fc see Table 3.

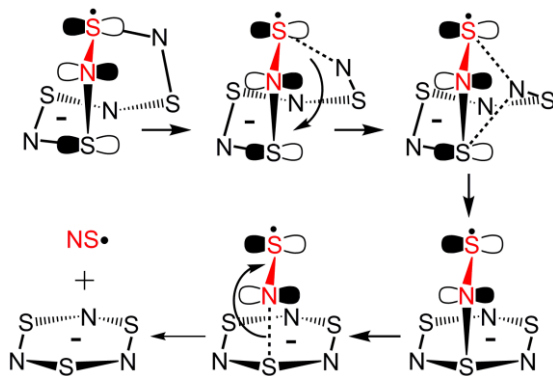
e. K_1 was fixed at a high value after considerable testing of alternatives; K_2 is a dependent variable.

Chemical Mechanisms for the Interconversion of S₄N₄ and [S₃N₃]⁻. The possible mechanisms for the interconversion of S₄N₄ and [S₃N₃]⁻ are discussed in the light of the detailed

kinetic data provided by the digital simulations of the CVs. We start by considering the decomposition of $[\text{S}_4\text{N}_4]^{-\bullet}$, which obeys first-order kinetics and is not influenced by the concentration of S_4N_4 . The previously reported^{3c} activation energy for this decomposition of $47 \pm 4 \text{ kJ mol}^{-1}$, along with our new value in CH_2Cl_2 of $62 \pm 2 \text{ kJ mol}^{-1}$ is consistent with a vibrationally-induced 1,3 nitrogen shift mechanism (Scheme 3) similar to what has been invoked to explain ring contractions for a variety of S,N heterocycles, i.e., dithiatetrazocine radical anions (**3**)¹² and trithiatetrazocines ($E_A = 67 \pm 4 \text{ kJ mol}^{-1}$),^{46a} as well as the exchange processes that occur in bicyclic CN_5S_3 ($E_A = 84 \pm 4 \text{ kJ mol}^{-1}$)^{46b-d} and $[\text{S}_4\text{N}_5]^+$ cages.⁴⁷ The recent investigation of the photochemical activation of S_4N_4 in argon matrices identified three intermediates, including a six-membered S_3N_3 ring carrying an exocyclic $-\text{N}=\text{S}$ group analogous to the proposed intermediate $[\text{cyclo-S}_3\text{N}_3-\text{N}=\text{S}]^{-\bullet}$ (PBE1PBE/(aug)cc-pVTZ calculated structure, Fig. S12) shown in Scheme 3 (bottom right).^{11,48} Interestingly, our analysis indicates that the conversion shown in Eqn 7 has an equilibrium constant of ca. 10^6 , indicating that a significant amount of $[\text{NS}]^{\bullet}$ must be present at the electrode surface. However, the $[\text{NS}]^{\bullet}$ radical is expected to be EPR-silent in condensed phases^{3h} and it was not observed in our EPR investigations.



Scheme 3. Formation of $[\text{S}_3\text{N}_3]^{-\bullet}$ and $[\text{NS}]^{\bullet}$ from $[\text{S}_4\text{N}_4]^{-\bullet}$ by a sigmatropic 1,3 nitrogen shift mechanism.



With respect to the (re)oxidation of $[\text{S}_3\text{N}_3]^-$, it is evident that the purported $[\text{S}_3\text{N}_3]^\bullet$ radical reverts rapidly to S_4N_4 . The kinetics demonstrate that decomposition may follow either a first-order or second-order pathway. For the first-order case, elimination of $[\text{NS}]^\bullet$ from $[\text{S}_3\text{N}_3]^\bullet$ would produce S_2N_2 .¹ It has been predicted that S_2N_2 in the presence of nucleophiles or reducing agents will rapidly form S_4N_4 .² Direct recombination of $[\text{NS}]^\bullet$ with $[\text{S}_3\text{N}_3]^\bullet$ is equally plausible given the evidence from the voltammetry study for a second-order recombination path along with the value of K_{eq1} which indicates that the concentration of $[\text{NS}]^\bullet$ is appreciable. We note that the intermediates *cyclo*- $\text{S}_3\text{N}_3\text{-N=S}$ and *cyclo*- $\text{S}_3\text{N}_3\text{-S}\equiv\text{N}$ identified by Zibarev *et al.* upon photochemical excitation may afford a direct pathway for the recombination of $[\text{NS}]^\bullet$ with $[\text{S}_3\text{N}_3]^\bullet$ via concerted reactions between their respective π systems.¹¹ Dimerization of $[\text{NS}]^\bullet$ is expected to lead to S_2N_2 , although Mawhinney and Goddard determined that in the gas phase the only such product is the linear NS-SN .⁴⁹ Thus several paths might well operate simultaneously for the conversion of $[\text{S}_3\text{N}_3]^\bullet$ to S_4N_4 .

The Electronic Structure of $[\text{S}_3\text{N}_3]^\bullet$. The electronic structure of $[\text{S}_3\text{N}_3]^\bullet$ has most recently been examined by us using density functional theory (DFT).¹⁴ The calculations fully supported a planar ring geometry with a $^2\text{A}_2$ ground state, in excellent agreement with the previous Hartree-Fock and CI calculations employing basis sets of minimal and double-zeta quality.¹⁵ The radical has C_{2v} symmetry but the geometrical distortions are very small when the optimized structure is contrasted with that of the diamagnetic D_{3h} symmetric $[\text{S}_3\text{N}_3]^-$ anion.⁴ The symmetry lowering upon detachment of an electron is readily understood by noting that the highest occupied molecular orbitals of $[\text{S}_3\text{N}_3]^-$ form an e'' symmetric degenerate pair. Thus, the radical undergoes a first-order Jahn-Teller distortion to displace the nuclei to new equilibrium positions of lower

symmetry, causing a splitting of the e'' level to two orbitals which transform as b_1 and a_2 in the C_{2v} point group.

The ground state electronic configuration of $[S_3N_3]^*$ is $\dots(5b_1)^2(3a_2)^1(6b_1)^0\dots$ based on the occupation of the orbitals in the Kohn-Sham reference determinant.¹⁴ However, the energy separation of the highest doubly and singly occupied orbitals is found to be only 0.01 Hartrees. This is not entirely unexpected considering that the $5b_1$ and $3a_2$ orbitals originate from the initially degenerate pair and that the molecular framework is very close to being of higher D_{3h} symmetry. It is therefore probable that the lowest 2B_1 state with a configuration $\dots(3a_2)^2(5b_1)^1(6b_1)^0\dots$ is energetically similar to the 2A_2 state and that the DFT calculation converged to one of the two possibilities by coincidence. Since DFT is in general not the method of choice to examine the properties of wave functions, we decided to conduct a thorough analysis of the ground state of $[S_3N_3]^*$ using a variety of *ab initio* methods.

The first signs of the peculiarities in the ground state wave function of $[S_3N_3]^*$ are observed in HF single point calculations which, even when started from the DFT optimized geometry, do not converge after 120 iterations (Gaussian) or converge to a highly improbable 2A_1 state (Molpro). Enforcing the symmetry of the wave function to be A_2 helps in both cases after which the HF calculations converge to the same solution as found using DFT. However, an analysis of the HF SCF iterations shows that the convergence problem is not initiated by two close-lying electronic states of different symmetry but rather two close-lying configurations belonging to the same A_2 representation of the C_{2v} point group. Hence, we conclude that the ground state wave function of $[S_3N_3]^*$ appears to be multideterminantal in character. This was confirmed by conducting CAS calculations; MP2 and CCSD calculations were also performed for comparative purposes.

The [3,3]-CAS optimizations unequivocally established that the ground state of $[\text{S}_3\text{N}_3]^*$ has $^2\text{A}_2$ symmetry; the optimized structure is also in good agreement with the DFT results. The CI vector coefficients indicate that the ground state wave function is a linear combination of five Slater determinants which form two configurations: the “closed shell doublet” configuration $(5b_1)^2(3a_2)^1(6b_1)^0 - (5b_1)^0(3a_2)^1(6b_1)^2$ and the “doublet triradical” configuration $(5b_1)^1(3a_2)^1(6b_1)^1$. The latter configuration is a linear combination of three Slater determinants differing only with respect to the spin state of the electrons ($1/2, -1/2, 1/2$; $1/2, 1/2, -1/2$ and $-1/2, 1/2, 1/2$) thereby ensuring that the wave function is a true eigenstate of both S_z and S^2 operators. The most important configurations in the ground state wave function of $[\text{S}_3\text{N}_3]^*$ are depicted in Figure 11 along with the pictures of frontier orbitals.

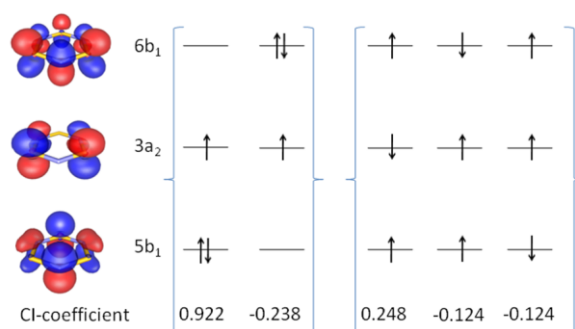


Figure 11. Frontier MOs (isosurface value ± 0.05) and leading configurations in the wave function of $[\text{S}_3\text{N}_3]^*$.

The wave function analysis shows that the doublet $^2\text{A}_2$ state of $[\text{S}_3\text{N}_3]^*$ is considerably more complex than what can be inferred from the DFT result alone: the near degeneracy of the $5b_1$, $3a_2$ and $6b_1$ orbitals allows three electrons to be distributed in three orbitals giving rise to a small triradical component in the wave function. The triradical character in $[\text{S}_3\text{N}_3]^*$ is sufficiently small to allow its treatment with modern exchange-correlation functionals and, hence, its presence remains unnoticed within the density functional formalism of electronic structure theory.

Triradicals with an open-shell doublet ground state have been of increasing experimental and theoretical interest during recent years⁵⁰ and $[\text{S}_3\text{N}_3]^*$ represents an interesting addition to the growing continuum of such systems. Since the ground state wave function of $[\text{S}_3\text{N}_3]^*$ is dominated by the closed-shell doublet configuration, it is not a true triradical species but can be best viewed as a *triradicaloid*. This is also evident from the calculated (adiabatic) doublet-quartet splitting which is as large as -120 kJ mol^{-1} . The electronic structure of $[\text{S}_3\text{N}_3]^*$ can therefore be contrasted to that of S_2N_2 in which the energetic proximity of the highest occupied (HOMO) and the lowest unoccupied molecular orbital (LUMO) induces a small but nevertheless significant singlet diradical character to the wave function.⁵¹

As in the case of S_2N_2 ,⁵¹ the failure in Hartree-Fock to describe the electronic structure of $[\text{S}_3\text{N}_3]^*$ is best seen when calculating molecular properties. For example, the vibrational frequencies of $[\text{S}_3\text{N}_3]^*$ show differences up to 300 cm^{-1} when the HF and DFT values are compared. It is interesting to note that MP2 suffices much better and predicts harmonic vibrational frequencies in reasonable qualitative and quantitative agreement with CCSD and DFT. However, the above does not hold for the band intensities since the most intense IR-transition at the MP2 level of theory –the lowest b_2 symmetric normal mode– has practically no intensity when the calculations are done using either density functional or coupled cluster methods. The failure of MP2 in describing $[\text{S}_3\text{N}_3]^*$ is also apparent from the calculated natural orbital occupation numbers (NOONs), which show one value significantly higher than two (2.13) and one much lower than zero (-0.16). The presence of negative NOONs in the MP2 wave function has been found to be highly indicative of the need for a multiconfigurational description of the system.⁵² In addition, the [3,3]-CAS NOON for the $6b_1$ orbital is 0.21 but the MP2 value is significantly lower, 0.04, giving a clear sign of the poor description of the frontier orbitals within

the latter method. However, the CAS calculation used a minimum active space which is significantly smaller than the full valence space generally required to obtain essentially converged orbital occupancies. Hence, in view of the minor triradical character in $[\text{S}_3\text{N}_3]^+$, the orbital occupation numbers calculated from the CCSD wave function should be considered the most accurate. Rather expectedly, all NOONs are found to be between 0 and 2 at the CCSD level, and the calculated occupations for the $5b_1$, $3a_2$ and $6b_1$ frontier orbitals are 1.88, 0.96 and 0.13, respectively, in good qualitative agreement with the CAS CI-vector coefficients. However, it is not obvious what effect triradicaloid character in the ground state wavefunction of $[\text{S}_3\text{N}_3]^+$ might have on the EPR behavior of this elusive species (if any).

Conclusions

The SEEPR technique, used in conjunction with isotopic labeling, is shown to be an effective tool for the identification of transient binary S,N radicals. Investigations of the nature of the interconversion between S_4N_4 and $[\text{S}_3\text{N}_3]^-$ have revealed that the primary electron-transfer product for S_4N_4 decays with first-order kinetics. The decay of the primary electron-transfer product for $[\text{S}_3\text{N}_3]^-$ is less straightforward and may follow either first or second-order kinetics. In either scenario, a significant role may be played by the EPR-silent $[\text{NS}]^+$ radical. SEEPR studies on ^{15}N and ^{33}S isotope-labeled S_4N_4 provide compelling confirmation of the identity of $[\text{S}_4\text{N}_4]^+$. However, it was not possible to detect $[\text{S}_3\text{N}_3]^+$ by applying the SEEPR technique to the oxidation of the corresponding anion $[\text{S}_3\text{N}_3]^-$, confirming previous reports for the non-observation of this species by EPR spectroscopy. [3,3]-CAS calculations unequivocally established that the ground state of $[\text{S}_3\text{N}_3]^+$ has distinct triradicaloid character.

Acknowledgments. Financial support from the Natural Sciences and Engineering Research Council-Canada (R.T.B. and T.C.), the Albert Ingenuity Fund (T.L.R.) and the Academy of

Finland (H.M.T.) is gratefully acknowledged. We thank the NSERC for the purchase of the EPR spectrometer, and the University of Lethbridge for the potentiostat. We would also like to thank Drs. Stephen Feldberg; Manfred Rudolph and an anonymous referee for help with the digital simulations and Dr. Keith Preston for advice on EPR spectra of $[\text{S}_3\text{N}_3]^+$.

Supporting Information Available: Crystallography details for $[\text{PPN}][\text{S}_3\text{N}_3\cdot\text{HOCH}_3]$ (Fig. S1, Table S1); CV conc. dep. for red. of S_4N_4 (Table S2); CV conc. dep. for ox. of $[\text{S}_3\text{N}_3]^-$ (Table S3); EPR spectrum of $\text{S}_4\text{N}_4^{\cdot-}$ at RT (Fig. S2); First-order rate constants vs. temp. for $[\text{S}_4\text{N}_4]^{\cdot-}$ (Table S4); Simulated EPR spectra for $[\text{S}_3\text{N}_3]^+$ (Fig. S3); First-order rate constants vs. temp. for $[\text{S}_4\text{N}_4]^{\cdot-}$ (Fig. S4); Half-lives vs. temp. for $[\text{S}_4\text{N}_4]^{\cdot-}$ (Fig. S5); Plot of $\ln k$ versus $1/T$ for S_4N_4 (Fig. S6); Exptl. and simulated CF for S_4N_4 (Fig. S7); Parameters from simulating the $\text{S}_4\text{N}_4^{-1/0}$ couple (Table S5); Sensitivity of $[\text{S}_3\text{N}_3]^-$ towards oxygen; CVs for oxidation of $[\text{S}_3\text{N}_3]^-$ (Fig. S8); Exptl. and simulated CVs for $[\text{Cp}_2\text{Co}][\text{S}_3\text{N}_3]$ (Fig. S9); Exptl. and simulated CVs for $[\text{PPN}][\text{S}_3\text{N}_3]$ (Fig. S10); Parameters from simulating the $[\text{S}_3\text{N}_3]^{-/0}$ couple (Table S6); Half-life for a second order reaction; PBE1PBE/(aug)cc-pVTZ geometry for a face-to-face dimer of $[\text{S}_3\text{N}_3]^+$ (Fig. S11). PBE1PBE/(aug)cc-pVTZ geometry of $[\text{cyclo-S}_3\text{N}_3\text{-N=S}]^{\cdot-}$ (Fig. S12). This material is available free of charge via the Internet at <http://pubs.acs.org>.

References and Notes

- (1) Chivers, T. *A Guide to Chalcogen-Nitrogen Chemistry*; World Scientific Publishing Co.: Singapore, 2005.
- (2) Oakley, R. T. *Prog. Inorg. Chem.* **1988**, *36*, 299-391.
- (3) (a) Chapman, D.; Massey, A. G. *Trans. Faraday Soc.* **1962**, *58*, 1291-1299. (b) Meinzer, R. A.; Pratt, D. W.; Myers, R. J. *J. Am. Chem. Soc.* **1969**, *91*, 6623-6625. (c) Williford, J. D.; VanReet, R. E.; Eastman, M. P.; Prater, K. B. *J. Electrochem. Soc.* **1973**, *120*, 1498-

1501. (d) Hojo, M. *Bull. Chem. Soc. Jpn.* **1980**, *53*, 2856-2860. (e) Chivers, T.; Hojo, M. *Inorg. Chem.* **1984**, *23*, 1526-1530. (f) Tweh, J. W.; Turner, A. G. *Inorg. Chim. Acta* **1981**, *48*, 173-177. (g) Preston, K. F.; Sutcliffe, L. H. *Mag. Res. Chem.* **1990**, *28*, 189-204. (h) Tanaka, K.; Yamabe, T.; Tachibana, A.; Kato, H.; Fukui, K. *J. Phys. Chem.* **1978**, *82*, 2121-2126. (i) Chung, G.; Lee, D. *J. Mol. Struct.* **2002**, *582*, 85-90. (j) Scherer, W.; Spiegler, M.; Pedersen, B.; Tafipolsky, M.; Hieringer, W.; Reinhard, B.; Downs, A. J.; McGrady, G. S. *Chem. Commun.* **2000**, 635-636. (k) Villena-Blanco, M.; Jolly, W. L. *Inorg. Synth.* **1967**, *9*, 98-102. (l) Maaninen, A.; Siivari, J.; Laitinen, R. S.; Chivers, T. *Inorg. Synth.* **2002**, *33*, 196-199.
- (4) (a) Bojes, J.; Chivers, T. *J. C. S. Chem. Comm.* **1977**, 453-454. (b) Bojes, J.; Chivers, T.; Drummond, I.; MacLean, G. *Inorg. Chem.* **1978**, *17*, 3668-3672. (c) Bojes, J.; Chivers, T. *Inorg. Chem.* **1978**, *17*, 318-321. (d) Chivers, T.; Laidlaw, W. G.; Oakley, R. T.; Trsic, M. *J. Am. Chem. Soc.* **1980**, *102*, 5773-5781. (e) Bojes, J.; Chivers, T.; Oakley, R. T.; Womershäuser, G.; Schnauber, M. *Inorg. Synth.* **1989**, *25*, 30-35. (f) Jones, R.; Kelly, P. F.; Williams, D. J.; Woollins, J. D. *Polyhedron*, **1987**, *6*, 1541-1545. (g) Bojes, J.; Chivers, T.; Laidlaw, W. G.; Trsic, M. *J. Am. Chem. Soc.* **1979**, *101*, 4517-4522.
- (5) Gillespie, R. J.; Kent, J. P.; Sawyer, J. F. *Inorg. Chem.*, **1981**, *20*, 3784-3799.
- (6) Gillespie, R. J.; Kent, J. P.; Sawyer, J. F.; Slim, D. R.; Tyrer, J. D. *Inorg. Chem.* **1981**, *20*, 3799-3812.
- (7) (a) Chandra, H.; Rao, D. N. R.; Symons, M. C. R. *J. Chem. Soc. Dalton Trans.* **1987**, 729-732. (b) Müller, U.; Conradi, E.; Demant, U.; Dehnicke, K. *Angew. Chem. Int. Ed.* **1984**, *23*, 237-238.

- (8) Cordes, A. W.; Marcellus, C. G.; Noble, M. C.; Oakley, R. T.; Pennington, W. T. *J. Am. Chem. Soc.*, **1983**, *105*, 6008-6012.
- (9) Brown, O. R. *J. Electroanal. Chem.* **1972**, *34*, 419-423.
- (10) Fritz, H. P.; Bruchhaus, R.; Mews, R.; Höfs, H.-U. *Z. Anorg. Allg. Chem.* **1985**, *525*, 214-220.
- (11) Pritchina, E. A.; Gritsan, N. P.; Zibarev, A. V.; Bally, T., *Inorg. Chem.* **2009**, DOI: 10.1021/ic802145x.
- (12) Boéré, R. T.; Bond, A. M.; Chivers, T.; Feldberg, S. W.; Roemmele, T. L. *Inorg. Chem.* **2007**, *46*, 5596-5607.
- (13) (a) Webster, R. D.; Bond, A. M.; Coles, B. A.; Compton, R. G. *J. Electroanal. Chem.* **1996**, *404*, 303-308. (b) Fiedler, D. A.; Koppenol, M.; Bond, A. M. *J. Electrochem. Soc.* **1995**, *142*, 862-867. (c) Neudeck, A.; Kress, L. *J. Electroanal. Chem.* **1997**, *437*, 141-156.
- (14) Boéré, R. T.; Tuononen, H. M.; Chivers, T.; Roemmele, T. L. *J. Organomet. Chem.* **2007**, *692*, 2683-2696.
- (15) (a) Lau, W. M.; Westwood, N. P. C.; Palmer, M. H. *J. Chem. Soc., Chem. Commun.* **1985**, 752-753. (b) Lau, W. M.; Westwood, N. P. C.; Palmer, M. H. *J. Am. Chem. Soc.* **1986**, *108*, 3229-3237.
- (16) (a) Banister, A. J.; Hansford, M. I.; Hauptman, Z. V.; Luke, A. W.; Wait, S. T.; Clegg, W. Jorgensen, K. A. *J. Chem. Soc. Dalton Trans.* **1990**, 2793-2802. (b) Lee, F. L.; Preston, K. F.; Williams, A. J.; Sutcliffe, L. H.; Banister, A. J.; S. T. Wait, *Magnet. Res. Chem.* **1989**, *27*, 1161-1165.

- (17) Jagg, P. N.; Kelly, P. F.; Rzepa, H. S.; Williams, D. J.; Woollins, J. D.; Wylie, W. J. *Chem. Soc., Chem. Commun.* **1991**, 942-944.
- (18) (a) Lipp, S. A.; Chang, J. J.; Jolly, W. M. *Inorg. Chem.* **1970**, 9, 1970-1973. (b) Jolly, W. L.; Maguire, K. D. *Inorg. Synth.* **1969**, 9, 102-111.
- (19) (a) Ruff, J. K.; Schlientz, W. J. *Inorg. Synth.* **1974**, 15, 84-87. (b) Blohm, M. L.; Gladfelter, W. L. *Inorg. Synth.* **1989**, 26, 286-289.
- (20) Stojanovic, R. S.; Bond, A. M. *Anal. Chem.* **1993**, 65, 56-64.
- (21) Bard, A. J.; Faulkner, L. R. *Electrochemical Methods: Fundamentals and Applications*, 2nd ed.; Wiley: New York, 2001.
- (22) Lide, D. R., *CRC Handbook of Chemistry and Physics*, 85th Edition. CRC Press, Boca Raton, 2004. Section 6, Page 203ff. See also Nath, J.; Dixit, A. P. *J. Chem. Eng. Data* **1984**, 29, 317-319 and Adam, H. H.; Baignie, B. D., Joslin, T. A. *J. Chem. Soc., Perkin Trans. 2* **1977**, 1287-1293.
- (23) (a) Rudolph, M. J. *Electroanal. Chem.* **2003**, 543, 23-39. (b) Rudolph, M. J. *J. Electroanal. Chem.* **2004**, 571, 289-307. (c) Rudolph, M. J. *Electroanal. Chem.* **2003**, 558, 171-176. (d) Rudolph, M. J. *Comput. Chem.* **2005**, 26, 619-632. (e) Rudolph, M. J. *Comput. Chem.* **2005**, 26, 1193-1204.
- (24) Bond, A. M. *Broadening Electrochemical Horizons*, Oxford University Press: New York, 2002.
- (25) Duling, D. R. *J. Mag. Res., Ser. B* **1994**, 104, 105-110.
- (26) Weil, J. A.; Bolton, J. R.; Wertz, J. E. *Electron Paramagnetic Resonance*; John Wiley & Sons: New York, 1994.

- (27) Crystal data for [PPN][S₃N₃·HOCH₃]: C₃₇H₃₄N₄OP₂S₃, $M_r = 708.80$, monoclinic space group Cc , $a = 15.5470(8)$, $b = 15.9857(8)$, $c = 14.6976(7)$ Å, $\beta = 109.363(1)^\circ$, $V = 3446.2(3)$ Å³, $Z = 4$, $T = 100(2)$ K, $\rho_{\text{calcd}} = 1.366$ g/cm³, $\mu(\text{Mo K}\alpha) = 0.345$ mm⁻¹, 22701 reflections collected (Θ range = $1.88\text{--}26.37^\circ$), 3521, unique ($R_{\text{int}} = 0.0411$), $R_1 = 0.0421$ [for 3241 reflections with $I > 2\sigma(I)$] and $wR_2 = 0.1118$ (for all data); GOF on $F^2 = 1.062$, completeness = 1.000.
- (28) Møller, C.; Plesset, M. S. *Phys. Rev.* **1934**, *46*, 618-622.
- (29) See, for example: Bartlett, R. J. *J. Phys. Chem.* **1989**, *93*, 1697-1708, and references therein.
- (30) Roos, B. O.; Taylor, P. R.; Siegbahn, P. E. M. *Chem. Phys.* **1980**, *48*, 157-173.
- (31) (a) Dunning, T. H. Jr. *J. Chem. Phys.* **1989**, *90*, 1007-1023. (b). Woon, D. E.; Dunning, T. H. Jr. *J. Chem. Phys.* **1993**, *98*, 1358-1371.
- (32) Gaussian 03, Revision C.02, Frisch, M. J.; Trucks, G. W.; Schlegel, H. B.; Scuseria, G. E.; Robb, M. A.; Cheeseman, J. R.; Montgomery, Jr., J. A.; Vreven, T.; Kudin, K. N.; Burant, J. C.; Millam, J. M.; Iyengar, S. S.; Tomasi, J.; Barone, V.; Mennucci, B.; Cossi, M.; Scalmani, G.; Rega, N.; Petersson, G. A.; Nakatsuji, H.; Hada, M.; Ehara, M.; Toyota, K.; Fukuda, R.; Hasegawa, J.; Ishida, M.; Nakajima, T.; Honda, Y.; Kitao, O.; Nakai, H.; Klene, M.; Li, X.; Knox, J. E.; Hratchian, H. P.; Cross, J. B.; Bakken, V.; Adamo, C.; Jaramillo, J.; Gomperts, R.; Stratmann, R. E.; Yazyev, O.; Austin, A. J.; Cammi, R.; Pomelli, C.; Ochterski, J. W.; Ayala, P. Y.; Morokuma, K.; Voth, G. A.; Salvador, P.; Dannenberg, J. J.; Zakrzewski, V. G.; Dapprich, S.; Daniels, A. D.; Strain, M. C.; Farkas, O.; Malick, D. K.; Rabuck, A. D.; Raghavachari, K.; Foresman, J. B.; Ortiz, J. V.; Cui, Q.; Baboul, A. G.; Clifford, S.; Cioslowski, J.; Stefanov, B. B.; Liu, G.;

- Liashenko, A.; Piskorz, P.; Komaromi, I.; Martin, R. L.; Fox, D. J.; Keith, T.; Al-Laham, M. A.; Peng, C. Y.; Nanayakkara, A.; Challacombe, M.; Gill, P. M. W.; Johnson, B.; Chen, W.; Wong, M. W.; Gonzalez, C.; and Pople, J. A.; Gaussian, Inc., Wallingford CT, 2004.
- (33) Molpro 2002.6 is a package of *ab initio* programs designed by Werner, H.-J. and Knowles, P.J. The authors are Amos, R.D.; Bernhardsson, A.; Berning, A.; Celani, P.; Cooper, D.L.; Deegan, M.J.O.; Dobbyn, A.J.; Eckert, F.; Hampel, C.; Hetzer, G.; Knowles, P.J.; Korona, T.; Lindh, R.; Lloyd, A.W.; McNicholas, S.J.; Manby, F.R.; Meyer, W.; Mura, M.E.; Nicklaß, A.; Palmieri, P.; Pitzer, R.; Rauhut, G.; Schütz, M.; Schumann, U.; Stoll, H.; Stone A. J.; Tarroni, R.; Thorsteinsson, T.; Werner, H.-J.
- (34) (a) Laaksonen, L. *J. Mol. Graph.* **1992**, *10*, 33-34. (b) Bergman, D. L.; Laaksonen, L.; Laaksonen, A. *J. Mol. Graph. Model.* **1997**, *15*, 301-306.
- (35) Banister, A. J.; Clegg, W.; Hauptman, Z. V.; Luke, A. W.; Wait, S. T. *J. Chem. Soc., Chem. Commun.* **1989**, 351-352.
- (36) The published synthesis of [PPN][S₃N₃] mentions recrystallization of the salt using identical solvents and conditions, but there is no mention of a solvent adduct (ref. 4d).
- (37) This redox couple was previously reported from [PPN][S₃N₃] in CH₂Cl₂/[ⁿBu₄N][BF₄] to be “reversible” and to occur at –0.17 V vs SCE (–0.31 V vs Fc⁺/Fc) in the same solvent (ref. 10). This difference in standard potential can readily be accounted for by differences in interfacial potentials from the use of the SCE reference electrode.
- (38) Cooper, J. B.; Bond, A. M. *J. Electroanal. Chem.* **1991**, *315*, 143-160.
- (39) Philip, I.; Kaifer, A. E. *J. Org. Chem.* **2005**, *70*, 1558-1564.

- (40) The calculated ^{33}S hfs constants for S_4N_4 are $a(^{33}\text{S}_{1,2}) = -0.65$ and $a(^{33}\text{S}_{3,4}) = 0.97$ mT *i.e.* one negative and one positive value; the original report (Ref. 14) unfortunately missed the positive sign for $a(^{33}\text{S}_{3,4})$.
- (41) Liebling, G. R.; McConnell, H. M. *J. Chem. Phys.* **1965**, *42*, 3931-3934.
- (42) (a) Freed, J.H., Fraenkel, G.K. *J. Chem. Phys.* **1962**, *37*, 1156-1157. (b) Sullivan, P.D., Bolton, J.R. *Adv. Mag. Resonance*, **1970**, *4*, 39.
- (43) (a) Appel, R.; Ruppert, I.; Milker, R.; Bastian, V. *Chem. Ber.* **1974**, *107*, 380-390. (b) Fritz, H. P.; Bruchhaus, R. *Electrochim. Acta*, **1984**, *29*, 947-950. (c) Domschke, G.; Mayer, R.; Bleisch, S.; Bartl, A.; Staško, A. *Mag. Res. Chem.* **1990**, *28*, 797-806.
- (44) For the EC and ECC classifications of heterogeneous electron transfer reactions (E) with coupled homogeneous chemical reactions (C), see chapter 12 of ref. 21, pp. 471-8.
- (45) (a) Evans, D. H. *Chem. Rev.* **1990**, *90*, 739-751. (b) Lerke, S. A.; Evans, D. H.; Feldberg, S. W. *J. Electroanal. Chem.* **1990**, *296*, 299-315. (c) Balducci, G.; Costa, G. *J. Electroanal. Chem.* **1993**^m *348*, 355-365. (d) González-Fernández, C. F.; García-Hernández, M. T.; Horno, J. *J. Electroanal. Chem.* **1995**, *395*, 39-44. (e) González-Fernández, M. T.; Castilla, J.; García-Hernández, C. F.; Horno, J. *J. Electroanal. Chem.* **1997**, *424*, 207-212. Note that in conventional settings of the square scheme, the reaction proceeds from top left to bottom right along both branches. The definitions used in Schemes 1 and 2 are designed for consistency with our prior treatments of the two components separately. Harmonization with the treatments in the cited references is readily accomplished by inverting the k_f and k_b terms for the left branch of the scheme.
- (46) (a) Boéré, R. T.; Cordes, A. W.; Oakley, R. T. *J. Am. Chem. Soc.* **1987**, *109*, 7781-7785. (b) Bestari, K. T.; Boéré, R. T.; Oakley, R. T. *J. Am. Chem. Soc.* **1989**, *111*, 1579-1584.

- (c) Boeré, R. T.; Oakley, R. T.; Shevalier, M. *J. Chem. Soc., Chem. Commun.* **1987**, 110-112. (d) Boeré, R. T.; Cordes, A. W.; Craig, S. L.; Graham, J. B.; Oakley, R. T.; Privett, J. A. *J. Chem. Soc., Chem. Commun.* **1986**, 807-808.
- (47) Bartetzko, R.; Gleiter, R. *Chem. Ber.* **1980**, *113*, 1138-1144.
- (48) The excited-state isomer of neutral tetrasulfur tetranitride [*cyclo*-S₃N₃-N=S] is a stable calculated gas-phase species by DFT methods (see Ref. 11). In our own work we have calculated the corresponding radical anion [*cyclo*-S₃N₃-N=S]^{-•} at the PBE1PBE/(aug)cc-pVTZ level of theory, the structure of which is somewhat less symmetrical than that of the neutral analog (Figure S12). However, we have not yet succeeded in tracing the path of the 1,3-N shift reaction shown in Scheme 3 computationally and therefore refrain from further discussion at this time. That such similar structure postulates are made for intermediates in photochemical (ref. 11) and electrochemical (this work) activation of the cage structure of S₄N₄ is, we believe, of significance.
- (49) Mawhinney R. C.; Goddard J. D. *Inorg. Chem.* **2003**, *42*, 6323-6337.
- (50) (a) Slipchenko, L. V.; Munsch, T. E.; Wenthold, P. G.; Krylov, A. I. *Angew. Chem., Int. Ed.* **2004**, *43*, 742-745. (b) Krylov, A. I. *J. Phys. Chem. A* **2005**, *109*, 10638-10645. (c) Koziol, L.; Winkler, M.; Houk, K. N.; Venkataramani, S.; Sander, W.; Krylov, A. I. *J. Phys. Chem. A* **2007**, *111*, 5071-5080.
- (51) (a) Tuononen, H. M.; Suontamo, R. S.; Valkonen, J.; Laitinen, R. S. *J. Phys. Chem. A* **2004**, *108*, 5670-5677. (b) Tuononen, H. M.; Suontamo, R. S.; Valkonen, J.; Laitinen, R. S.; Chivers, T. *J. Phys. Chem. A* **2005**, *109*, 6309-6317.
- (52) Gordon, M. S.; Schmidt, M. W.; Chaban, G. M.; Glaesemann, K. R.; Stevens, W. J.; Gonzalez, C. *J. Chem. Phys.* **1999**, *110*, 4199-4207.